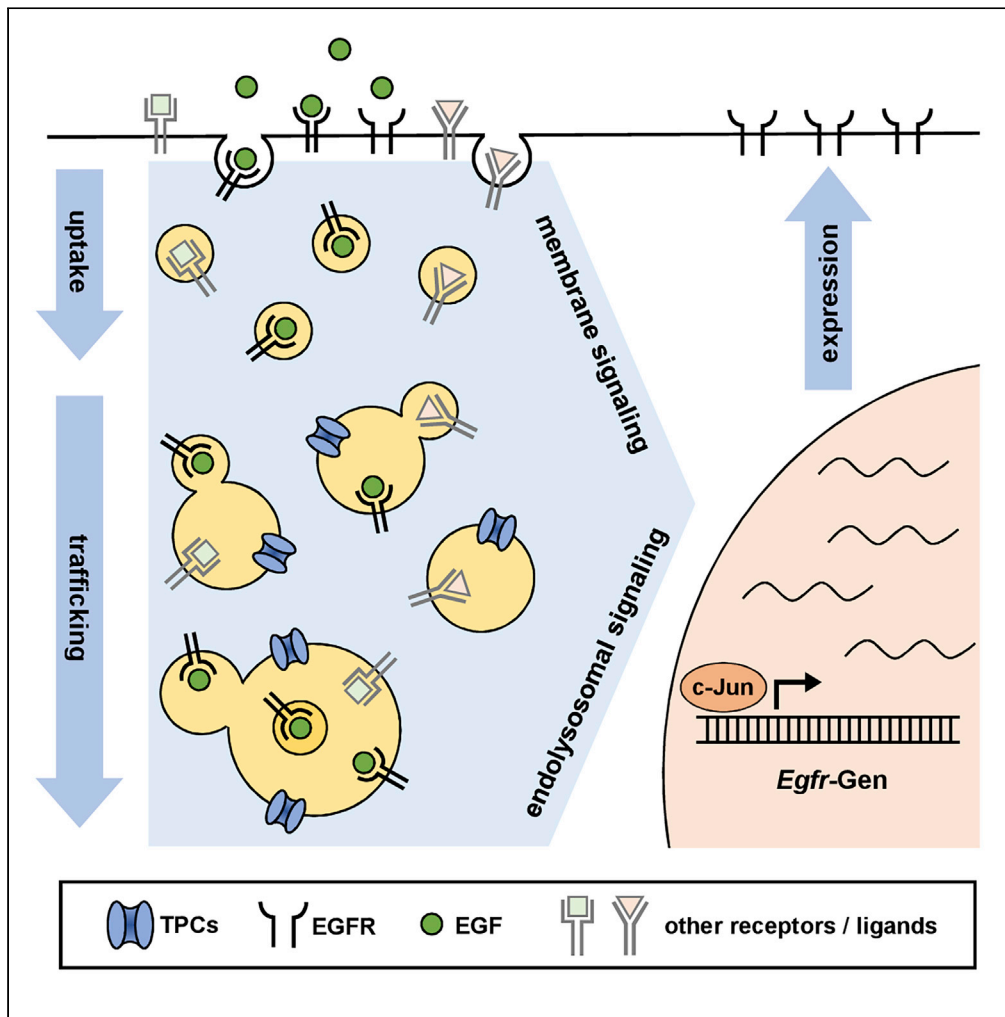


Article

Two-pore channels affect EGF receptor signaling by receptor trafficking and expression



Thomas Müller,
Sonja Grossmann,
Robert Theodor
Mallmann, Carolin
Rommel, Lutz
Hein, Norbert
Klugbauer

n.klugbauer@pharmakol.
uni-freiburg.de

HIGHLIGHTS

Two-pore channels
differently affect
intracellular trafficking of
EGF receptors

Deletion of TPCs prolongs
EGFR signaling in
endolysosomal platforms

TPCs affect expression of
EGFR downstream
signaling components

JNK signaling contributes
to increased EGFR
expression in TPC-
deficient cells

Müller et al., iScience 24,
102099
February 19, 2021 © 2021 The
Author(s).
[https://doi.org/10.1016/
j.isci.2021.102099](https://doi.org/10.1016/j.isci.2021.102099)



Article

Two-pore channels affect EGF receptor signaling by receptor trafficking and expression

Thomas Müller,¹ Sonja Grossmann,¹ Robert Theodor Mallmann,¹ Carolin Rommel,¹ Lutz Hein,¹ and Norbert Klugbauer^{1,2,*}

SUMMARY

Two-pore channels (TPCs) are key components for regulating Ca²⁺ current from endosomes and lysosomes to the cytosol. This locally restricted Ca²⁺ current forms the basis for fusion and fission events between endolysosomal membranes and thereby for intracellular trafficking processes. Here, we study the function of TPC1 and TPC2 for uptake, recycling, and degradation of epidermal growth factor receptor (EGFR) using a set of TPC knockout cells. RNA sequencing analysis revealed multiple changes in the expression levels of EGFR pathway-related genes in TPC1-deficient cells. We propose that a prolonged presence of activated EGFRs in endolysosomal signaling platforms, caused by genetic inactivation of TPCs, does not only affect EGFR signaling pathways but also increases *de novo* synthesis of EGFR. Increased basal phospho-c-Jun levels contribute to the high EGFR expression in TPC-deficient cells. Our data point to a role of TPCs not only as important regulators for the EGFR transportation network but also for EGFR-signaling and expression.

INTRODUCTION

Two-pore channels (TPCs) comprise a small family of ion channels with only two representatives in rodents and humans, TPC1 and TPC2. Structurally they are evolutionary intermediates between single-domain TRP and four-domain voltage-gated Na⁺ or Ca²⁺ channels (Galione, 2019; Jentsch et al., 2015; Patel, 2015). TPCs are located in membranes of the endolysosomal system and are assumed to play a crucial role for intracellular trafficking processes (Grimm et al., 2017; Marchant and Patel, 2015). As acidic compartments of the endolysosomal system constitute small Ca²⁺ stores, it can be assumed that TPCs form cytosolic Ca²⁺ entry pathways, which allow for a transient and locally restricted increase of Ca²⁺. This elevation of Ca²⁺ triggers fusion and fission events of endolysosomal membranes and thereby forms the basis for intracellular vesicle trafficking and sorting processes during protein uptake, recycling, and degradation (Grimm et al., 2014; Sakurai et al., 2015). So far, the function of TPCs has mostly been investigated by targeted deletion of single TPC genes in mice. TPC functions have been described in the context of receptor endocytosis, degradation, and recycling; of bacterial protein toxin uptake; and of entry and processing of virus particles (Castonguay et al., 2017; Grimm et al., 2014; Sakurai et al., 2015). Consequently, all these models resulted in distinct phenotypes such as development of fatty liver disease in the case of LDL receptor regulation, an impairment of toxin uptake and severity of intoxication, and endolysosomal trapping of virus particles and prevention of infection.

The epidermal growth factor receptor (EGFR) belongs to the ErbB family of growth factor receptors with intrinsic tyrosine kinase activity and is involved in key processes such as cell growth, differentiation, proliferation, and motility (Ceresa and Peterson, 2014). In many tumors EGFR is either upregulated or mutated and numerous recent therapeutic strategies aim at blocking oncogenic EGFR signaling (Shan et al., 2012; Tomas et al., 2014). EGFR signaling is initiated by ligand binding to receptors present at the cell surface, which triggers their dimerization and auto-phosphorylation. Activated receptors are internalized by clathrin-mediated (CME) or clathrin-independent endocytosis (CIE) (reviewed in Bakker et al., 2017). Although ligand binding and initiation of signal transduction occurs at the cell surface, activated EGFR is located for the longest period within endolysosomal membranes where EGFR signaling is still ongoing (Conte and Sigismund, 2016; Sousa et al., 2012; Vieira et al., 1996). The intracellular EGFR transportation network has

¹Institut für Experimentelle und Klinische Pharmakologie und Toxikologie, Fakultät für Medizin, Albert-Ludwigs-Universität Freiburg, Albertstr. 25, 79104 Freiburg, Germany

²Lead Contact

*Correspondence:

n.klugbauer@pharmakol.uni-freiburg.de

<https://doi.org/10.1016/j.isci.2021.102099>



been well studied over the last decades, and it was shown that ligand concentrations determine the preferential trafficking route of activated receptor (Sigismund et al., 2008). At low EGF concentrations, uptake of EGFRs primarily occurs by CME and EGFRs are transported via early and recycling endosomes back to the plasma membrane (Rappoport and Simon, 2009). At higher EGF concentrations, a saturation effect can be observed and increasing amounts of activated EGFRs are taken up by CIE and are routed via late endosomes to lysosomes for degradation (Bakker et al., 2017). In this context, earlier studies demonstrated a link between EGFR trafficking and TPCs, because deletion of TPC2 causes an accumulation of EGFR in endolysosomal compartments (Grimm et al., 2014; Sakurai et al., 2015).

Recent studies indicate that EGFR signaling occurs not only during surface localization (Sousa et al., 2012) but also after internalization of activated EGFR (Conte and Sigismund, 2016) (Wu et al., 2012). For example, transcriptional activity of the ERK1/2 pathway is directly affected by the localization of EGFR in the endolysosomal system (Sousa et al., 2012; Wu et al., 2012). Thus, analysis of EGFR uptake and EGFR trafficking allows one to uncover the potential roles of the endolysosomally localized TPCs within this transportation system. In this study, we took advantage of mouse embryonic fibroblast (MEF) and HeLa cells with single TPC knockouts, and also of a TPC1/2 double knockout to explore its consequences on EGFR signaling. We identify TPCs not only as key regulators for intracellular EGFR trafficking but also for controlling EGFR transcription and surface expression.

RESULTS

Fluorescence microscopy exemplifies an altered EGFR uptake and trafficking in TPC-deficient cells

TPCs play a crucial role for intracellular trafficking processes and affect receptor endocytosis, recycling, and degradation. In this study, we investigated the roles of TPCs for processing and signaling of the EGFR, a well-studied receptor for regulating cell growth not only under physiological but also under pathophysiological conditions. For this purpose, we used MEF cells derived from transgenic mouse lines with a targeted disruption of either TPC1 or TPC2, the only two members of rodent and human TPC family (Arndt et al., 2014; Grimm et al., 2014). Furthermore, a TPC1/2-double knockout MEF cell line was generated in this study by applying the CRISPR-Cas9 system as described in Supplemental information (Figure S1).

Initial studies were performed to compare the uptake of EGFR in wild-type and TPC-deficient MEF cells. Cells were incubated for 60 min with 200 ng/mL EGF labeled with Alexa 488. This high concentration favors CIE of the EGF-EGFR complex and initiates trafficking processes that are mainly linked to degradation routes (Sigismund et al., 2008). As a result, TPC-deficient cells internalized higher amounts of labeled EGF than wild-type cells (Figure 1: top panel). In comparison with single knockouts, TPC1/2 double knockouts demonstrated the highest accumulation of EGF. A Rab5 staining highlighting early endosomes did not indicate any differences in the distribution pattern of Rab5-positive compartments in wild-type and knockout cells (Figure 1: middle panel). However, TPC2 and TPC1/2 double knockouts showed numerous examples of co-localization of Rab5- and EGF-positive vesicles, whereas wild-type and TPC1-deficient MEF cells showed only a few (Figure 1: bottom panel and arrowheads in insets in C and D). A quantification of the area covered by EGF/Rab5-positive vesicles indicates significant differences between those groups (Figure S2). The values for wild-type and TPC1-deficient cells were $0.05\% \pm 0.02\%$ and $0.13\% \pm 0.05\%$, respectively. For TPC2 and TPC1/2 double knockouts coverage values were $0.34\% \pm 0.07\%$ and $0.36\% \pm 0.11\%$, respectively. These initial studies indicate that TPCs are involved in different ways in the uptake and intracellular trafficking of the EGF-EGFR complex.

Deletion of TPCs increases EGFR uptake

A fluorescence-activated cell sorting (FACS)-based method was applied to quantify the findings of the initial fluorescence microscopic approach. MEF cells were incubated with high concentrations of EGF-Alexa488 for 10 to 120 min and were subjected to subsequent FACS analysis. The fluorescence intensities correlated with the amount of incorporated EGF and were used to study the kinetics of EGF uptake and receptor trafficking. All Alexa 488 fluorescence histograms showed a rightward shift compared with untreated controls; this effect was strongest for TPC1/2 double knockouts (Figures 2A–2D). Interestingly, TPC2-deficient cells demonstrated the broadest signal distribution. The quantification of the fluorescence signal of all genotypes revealed a continuous increase of fluorescence over the entire experimental period of 120 min and clearly indicated higher values for the knockouts, in particular for the TPC1/2 double knockout (Figure 2E). The single MEF cell knockouts showed a 2- to 3-fold increase, and the double

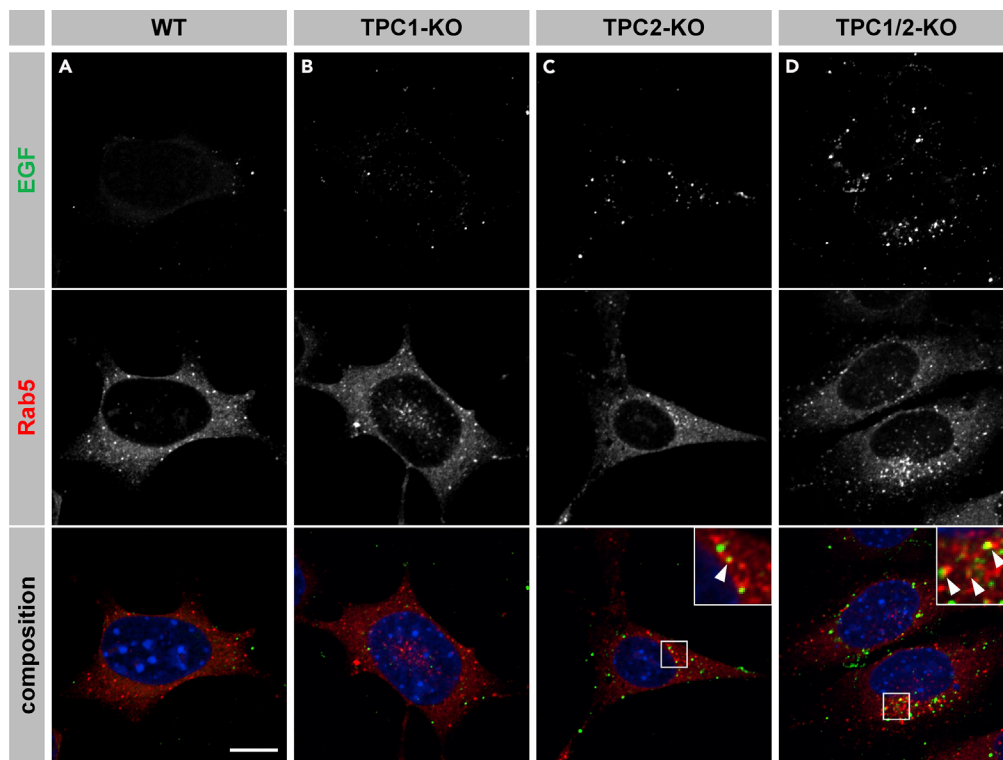


Figure 1. Representative fluorescence microscopic images of MEF cells after 60-min incubation with Alexa 488-labeled EGF

(A–D) (A) Wild-type, (B) TPC1-deficient, (C) TPC2-deficient, and (D) TPC1/2 double knockout MEF cells. Top panel, EGF-Alexa488 fluorescence; middle panel, immunofluorescence staining of Rab5-positive compartments; bottom panel, composition of EGF and Rab5 fluorescence signal together with DAPI staining. Insets in (C and D) indicate examples of EGF- and Rab5-positive vesicles (arrowheads). Scale bar, 10 μ m.

knockout showed a 4- to 6-fold increase over the entire experimental time frame. To generalize and to lay our conclusions on a broader basis we included wild-type and TPC1-deficient HeLa cells into our studies (Castonguay et al., 2017). The FACS analysis was performed in the same way as for MEF cells, and fluorescence histograms again showed a rightward shift when the cells were treated with EGF-Alexa488 (Figures 2F and 2G). The quantification of the fluorescence signals at 10 min, 30 min, and 60 min all resulted in a significant increase in TPC1-deficient HeLa cells when compared with wild-type cells (Figure 2H). In summary, the FACS-based quantification confirmed the observations made in the fluorescence microscopy studies and indicated a faster and appreciably higher uptake of EGF-Alexa488 in TPC-deficient cell lines.

To confirm that the above-mentioned effects were indeed caused by deletion of TPCs, we performed rescue experiments. Thus, single TPC knockout MEF cells were transfected either with the corresponding TPC-EGFP-encoding vector or with an EGFP vector as control. After 24 h, cells were stimulated with EGF-TexasRed for 2 h and subjected to FACS analysis. Only cells positive for expression of EGFP constructs were included in the analysis. Both the TPC1 and the TPC2 rescue experiments confirmed that the expression of corresponding TPC-EGFP vector recovered the wild-type phenotype of the MEF cells, i.e., a reduced uptake of EGF-TexasRed (Figure S3).

Lysosomal degradation does not contribute to observed TPC effects

Next, we checked for a possible lysosomal degradation and stability of EGF-Alexa488 conjugate by performing pulse-chase studies. MEF cells of all genotypes were incubated with EGF-Alexa488 for 1 h at 4°C followed by a washing step to remove any unbound fluorescence-labeled EGF. Afterward cells were incubated with non-labeled EGF at 37°C for 30 and 60 min. FACS analysis revealed no significant differences between the genotypes, when comparing fluorescence intensities after 30 and 60 min with initial values (Figure S4). As there was no decline in fluorescence intensities, degradation, inactivation, or outward

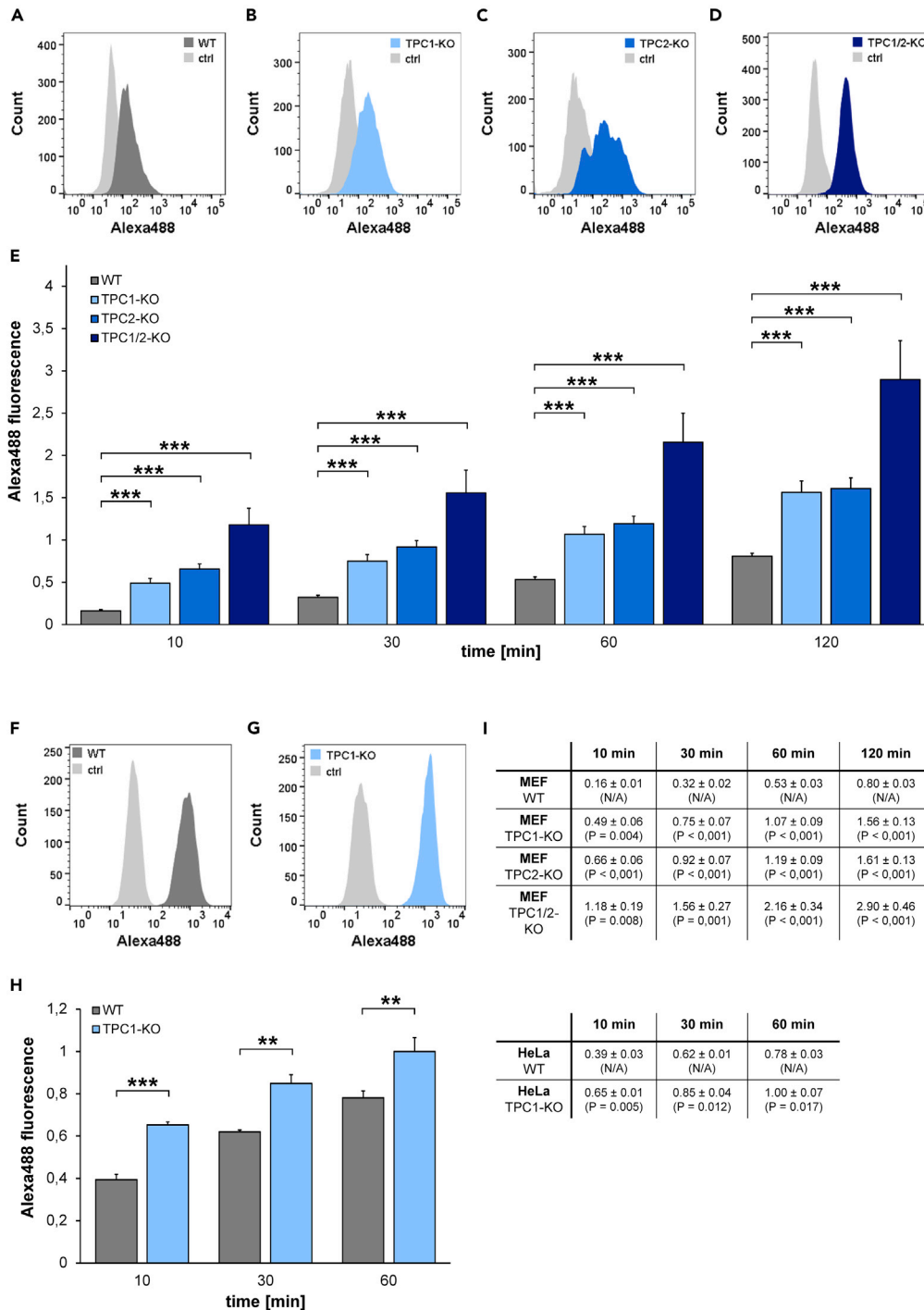


Figure 2. FACS analysis of EGF-Alexa488 uptake in MEF and HeLa cells

(A–D) Representative fluorescence histograms after 60-min incubation with 200 ng/mL EGF-Alexa488 at 37°C for wild-type (A), TPC1-deficient (B), TPC2-deficient (C), and TPC1/2-double knockout (D) MEF cells. Histograms of untreated cells are indicated in light gray and EGF-treated cells in dark gray (wild-type) or in blue colors (knockouts).

(E) Quantification of fluorescence signals for time points $t = 10$ min, $t = 30$ min, $t = 60$ min, and $t = 120$ min after incubation with EGF-Alexa488. Bar diagrams show mean values and standard errors of the median Alexa 488-fluorescence intensities normalized to an independent wild-type value at $t = 180$ min. Number of experiments is five ($n = 5$). Datasets were evaluated via ANOVA and Bonferroni post-hoc test ($***p \leq 0.01$).

Figure 2. Continued

(F and G) Representative fluorescence histograms after 60-min incubation with 200 ng/mL EGF-Alexa488 at 37°C for wild-type (F) and TPC1-deficient (G) HeLa cells. Histograms of untreated cells are indicated in light gray and EGF-treated cells in dark gray (wild-type) or in blue color (TPC1 knockout).

(H) Quantification of fluorescence signals for time points $t = 10$ min, $t = 30$ min, and $t = 60$ min and after incubation with EGF-Alexa488. Bar diagram shows mean values and standard errors of the median Alexa 488-fluorescence intensities normalized to highest values at $t = 60$ min. The number of experiments is three ($n = 3$). Datasets were evaluated via ANOVA and Bonferroni post-hoc test (** $p \leq 0.03$; *** $p \leq 0.01$).

(I) Data table showing the calculated fluorescence intensity values and p values.

transfer of the fluorophore can be excluded for at least 60 min. During the entire experiment, labeled EGF either remained within cells or was bound to the cellular surface rendering the occurrence of putative exocytotic processes during previously performed EGF uptake studies unlikely.

TPC-deficient cells express higher amounts of surface-accessible EGFR

Differences in EGFR endocytosis or degradation between wild-type and TPC-deficient MEF cells may also be caused by an altered expression level or membrane distribution of the EGFR. Therefore, EGF-Alexa488 binding experiments and immunoblot-based analyses of EGFR amounts were performed. MEF cells of all genotypes were incubated for 60 min with 200 ng/mL EGF-Alexa488 at 4°C and were evaluated by FACS analysis. As a result, all cells demonstrated a significant binding of labeled EGF (Figures 3A–3D). However, when comparing the different genotypes, we found an increased binding in the order wild-type, TPC1-KO (knockout), TPC2-KO, TPC1/2-doubleKO, highest for the double knockout (Figure 3E). Additionally, cell lysates from all MEF genotypes were analyzed by western blot and quantified using tubulin as loading control.

The results from these experiments were completely in line with those from the binding studies and indicated the same order of EGFR expression (Figures 4A and 4B). Thus the total amount of EGFR (western blot) as well as surface-accessible EGFR (binding studies) was significantly increased in TPC-deficient MEF cells and was the highest in TPC1/2-doubleKO. Additionally, we investigated EGFR expression in HeLa cells by immunoblot analysis (Figure 4C). The results from these studies indicated roughly a doubling of the EGFR levels in TPC1-deficient HeLa cells and were in line with data from the MEF cells (Figure 4D).

EGFR degradation follows the same kinetics in wild-type and TPC-deficient cells

EGFR levels were investigated by means of western blot analysis in the presence of the protein synthesis inhibitor cycloheximide (10 μ g/mL). This approach allows for a quantification of EGFR levels only depending on degradation, but not on *de novo* synthesis. Serum-starved MEF cells were exposed to 200 ng/mL EGF for up to 120 min, and EGFR levels were determined for each genotype. Control cells were stimulated with EGF in the absence of cycloheximide. As expected, initial EGFR levels varied between genotypes (wild-type [WT]: 100% \pm 19%, TPC1-KO: 455% \pm 25%, TPC2-KO: 572% \pm 21%, TPC1/2-KO: 549% \pm 18%) and were normalized to the same starting value to facilitate comparison of degradation kinetics. There were no statistically significant differences in degradation kinetics between wild-type and TPC-deficient MEF cells, indicating that the higher expression levels of EGFR in TPC-deficient cells are not caused by an impaired degradation process (Figure 5).

TPC-deficient cells show higher recovery rates

In the context of regenerative processes, two main routes, recycling of internalized receptor and *de novo* receptor synthesis, determine the amount of surface-accessible EGFR. To investigate the role of TPCs on these regenerative processes we established protocols that allowed quantifying EGFR surface expression and transcription levels. MEF cells were incubated with a high concentration of 200 ng/mL of non-labeled EGF at 4°C to saturate surface-expressed EGFR. After 1 h, non-labeled EGF was substituted by EGF-Alexa488, and cells were incubated for 10, 30, and 60 min at 37°C. Additionally, to quantify the amount of surface-expressed EGFR at starting time, cells were kept at 4°C for an additional hour with EGF-Alexa488. Quantification of the initial level of surface EGFR was determined by incubation of MEF cells with EGF-Alexa488 alone. Cells of all genotypes were handled in parallel and were analyzed by FACS. The 1-h receptor saturation with non-labeled EGF significantly reduced the subsequent binding of Alexa 488-labeled EGF to MEF cells in all genotypes. In contrast to wild-type cells, which showed a reduction of only 10%, all TPC-deficient cells demonstrated a much stronger drop down of fluorescence intensity (Figure 6A).

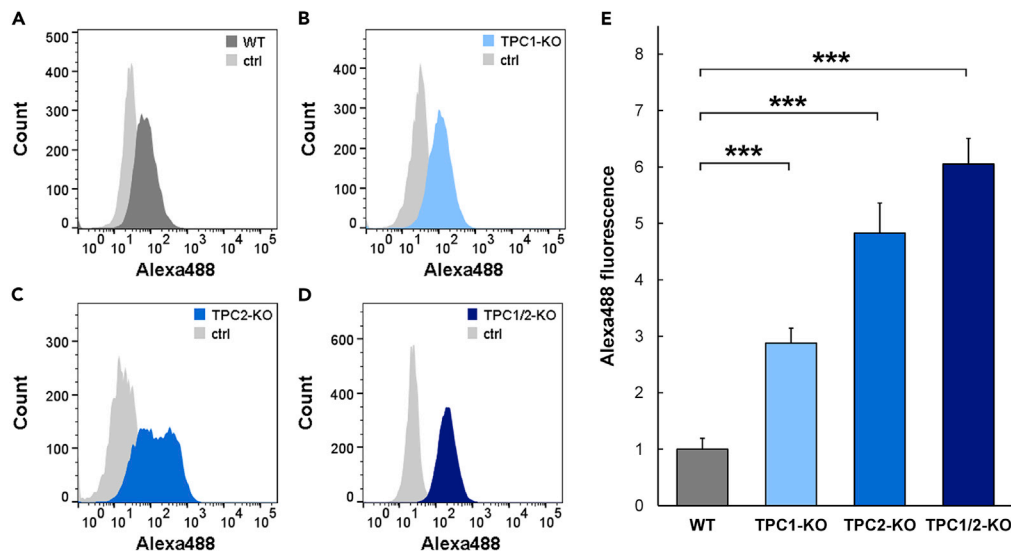


Figure 3. FACS analysis of EGF-Alexa488 binding to MEF cells

(A–D) Representative fluorescence histograms after 60-min incubation with 200 ng/mL EGF-Alexa488 at 4°C for wild-type (A), TPC1-deficient (B), TPC2-deficient (C), and TPC1/2-double knockout (D) MEF cells. Histograms of untreated cells are indicated in light gray and EGF-treated cells in dark gray (wild-type) or in blue colors (knockouts).

(E) Quantification of fluorescence signals after incubation with EGF-Alexa488 for 1 h. Bar diagram shows mean values and standard errors of the mean (SEM). Alexa 488-fluorescence intensities were normalized to an independent wild-type value. Number of experiments is ten (n = 10). Datasets were evaluated via ANOVA and Bonferroni post-hoc test (***)p ≤ 0.01). WT: 1.00 ± 0.20. TPC1-KO: 2.88 ± 0.26 (p = 0.007). TPC2-KO: 4.83 ± 0.53 (p < 0.001). TPC1/2-KO: 6.05 ± 0.45 (p < 0.001).

During the following regeneration period from 10 to 60 min, MEF cells of all genotypes showed an increased binding of EGF-Alexa488 (Figures 6A and 6B). Wild-type cells demonstrated only very moderate increases in fluorescence, but reached higher values after 1 h compared with control cells (cells incubated with labeled EGF only) (Figure 6B). All TPC-deficient cells showed a faster regeneration of surface-accessible EGFR. This effect was dependent on the type of TPC knockout and was the highest for TPC1/2-doubleKO (Figure 6B). For wild-type cells, recovery time was approximately 30 min. TPC1-deficient cells did not reach initial levels even after a regeneration window of 60 min. TPC2- and TPC1/2-doubleKO cells only achieved about 60% of recovery after 1 h when compared with starting levels. In view of the absolute amounts of surface-accessible EGFR, all TPC-deficient cells recovered significantly higher EGFR levels than wild-type cells.

Egfr mRNA levels are increased in TPC-deficient cells

The high concentration of 200 ng/mL of EGF favors the non-canonical endosomal and receptor degradation route and points to a *de novo* receptor synthesis as the main mechanism for receptor recovery. Therefore, we analyzed *Egfr* transcript levels of all cells by real-time PCR (qPCR). All TPC-deficient cells demonstrated higher transcript levels compared with wild-type cells, in the same order as observed in previous experiments with highest values for TPC1/2-doubleKO showing an about 12-fold increase (Figure S5). Thus, regeneration and qPCR studies clearly indicate that *de novo* synthesis of EGFR in TPC-deficient cells is the major mechanism responsible for the higher surface expression of EGFR.

RNA sequencing analysis confirms EGFR upregulation and highlights numerous transcriptional changes in EGFR-linked pathways in TPC1-deficient MEF cells

The high expression of EGFR in TPC-deficient MEF cells led us to investigate the consequences of a TPC1 deletion in EGFR-linked pathways. First, RNA sequencing (RNA-seq) coverage tracks for *Egfr* in wild-type compared with TPC1 knockout cells indicated a more than 3-fold increase of *Egfr* transcripts in TPC1-KO cells (Figure S6A). These results correspond perfectly to our western blot, qPCR, and FACS data and further substantiates that TPC deficiency causes a strongly increased *Egfr* expression in MEF cells (Figure S6B). Second, we took advantage of our RNA-seq data and studied the transcriptional changes of major

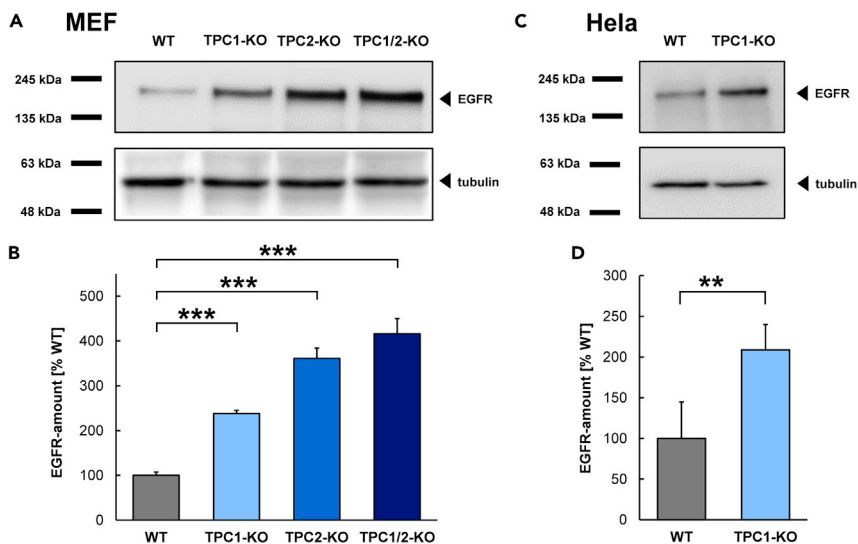


Figure 4. Quantification of EGFR amounts in MEF and HeLa cells by western blot analysis

(A) Representative western blots of wild-type and TPC-KO MEF cell lysates. Top panel, EGFR; bottom panel, tubulin as control.

(B) Quantification of EGFR protein amounts from five independent western blots ($n = 5$). Bar diagram shows mean values and standard errors of the luminescence signal when compared with wild-type. Datasets were evaluated via ANOVA and Bonferroni post-hoc test ($***p \leq 0.01$). WT: $100\% \pm 17\%$. TPC1-KO: $238\% \pm 7\%$ ($p = 0.005$). TPC2-KO: $361\% \pm 23\%$ ($p < 0.001$). TPC1/2-KO: $416\% \pm 32\%$ ($p < 0.001$).

(C) Representative western blot analysis of wild-type and TPC1-KO HeLa cell lysates. Top panel, EGFR; bottom panel, tubulin as control.

(D) Quantification of EGFR protein amounts from five independent western blots ($n = 5$). Bar diagram shows mean values and standard errors of the luminescence signals when compared with wild-type. Datasets were evaluated via ANOVA and Bonferroni post-hoc test ($**p \leq 0.03$).

EGFR pathway genes in TPC1-deficient cells. Our analysis focused on pathways involved in cytoskeletal regulation, endocytosis, apoptosis, and protein synthesis and on expression of relevant transcription factors (Table S1). To provide a comprehensive overview, RNA-seq data were transferred into a scheme highlighting the changes of gene expression involved in EGFR pathways (Figure 7). It is evident from this scheme that deletion of TPC1 affects EGFR-dependent pathways in multiple ways.

TPC-deficient cells exhibit prolonged EGFR signaling

Binding of EGF to EGFR results in receptor auto-phosphorylation and initiation of its kinase activity. In accordance with the high surface expression and regeneration of EGFR in MEF cells deficient for TPCs, we investigated possible consequences for EGFR signaling. MEF cells of all genotypes were stimulated with 200 ng/mL EGF for 1, 3, 5, and 10 min and lysed and subjected to SDS-PAGE. Western blots were evaluated for total amounts of ERK1/2, for phosphorylated ERK1/2 (pERK1/2), and for tubulin. Initial ERK1/2 and pERK1/2 levels were determined initially in the absence of EGF. At the beginning of the experiment ($t = 0$) pERK1/2 was hardly detectable in all probes (Figure 8 and Table S2). EGF stimulation resulted in a fast and transient ERK1/2 phosphorylation from the first to the fifth minute, which was comparable in wild-type and TPC-deficient cells. However, differences emerged after 10 min demonstrating a drop of pERK1/2 compared with the initial levels in wild-type cells, whereas all TPC-deficient cells still showed elevated pERK1/2 levels (Figure 8 and Table S2). As a control, basal ERK1/2 levels were measured for the entire experimental period. Values for ERK1/2 were stable, indicating that availability of non-phosphorylated ERK1/2 was constant for each time point. In summary, the data indicate that deletion of TPCs in MEF cells caused a prolonged activation of EGFR and ERK1/2 signaling.

TPC-deficient MEF cells demonstrate higher basal c-Jun phosphorylation levels than wild-type cells

Basal expression of EGFR is mainly regulated by transcription factor SP1, which is typically present in the nucleus in constant amounts. However, several studies indicate that EGFR transcription is further regulated by MAP

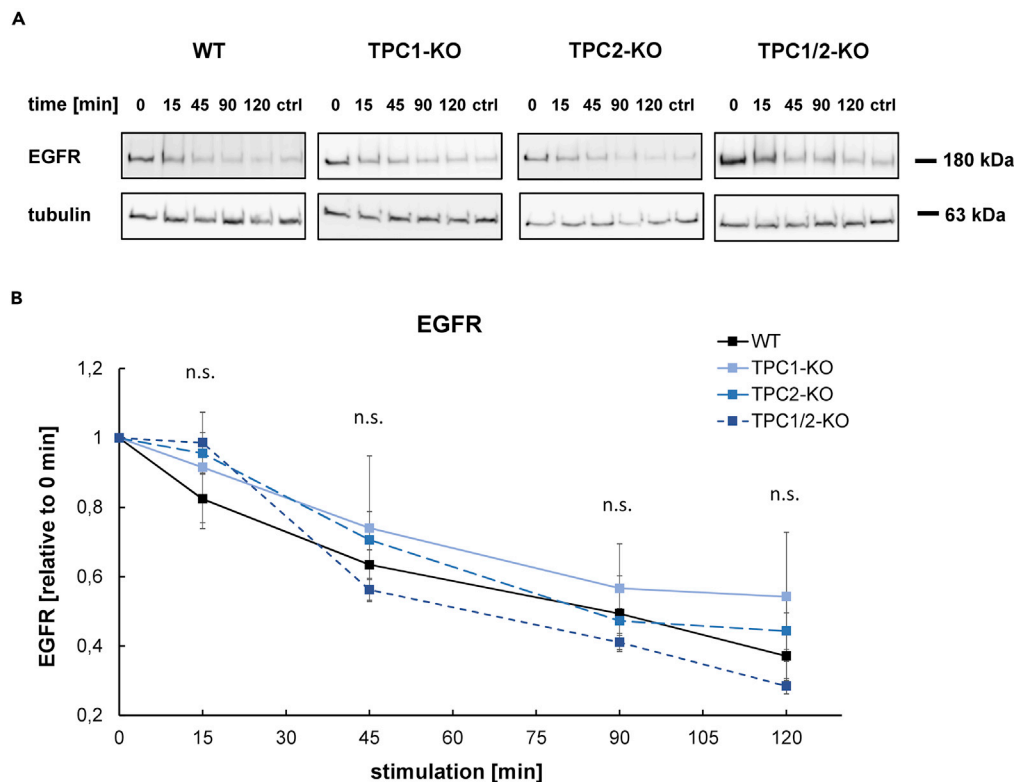


Figure 5. Degradation of EGFR in the presence of a protein synthesis inhibitor

(A) Representative western blots of wild-type and TPC-deficient MEF cell lysates after different time points of stimulation with 200 ng/mL EGF in the presence of cycloheximide. Control cells were treated with EGF for 120 min in the absence of cycloheximide. Top panel, EGFR; bottom panel, tubulin as control.

(B) Quantification of EGFR protein amounts from four independent western blots (n = 4). Diagram shows decrease in EGFR amount over time in relation to starting levels (0 min). Datasets were evaluated via ANOVA.

kinase-activated transcription factor c-Jun (Fang et al., 2014; Mialon et al., 2005; Weston et al., 2004). Therefore, we investigated phosphorylation of c-Jun in wild-type and TPC-deficient cells under basal and EGF-stimulated conditions. Phospho-specific c-Jun antibodies already indicated a strong phosphorylation of c-Jun under basal non-stimulated conditions in TPC1-, TPC2-, and TPC double knockout cells (Figures 9A and 9B). These differences were significant between wild-type and each of the deletion mutants. Stimulation by EGF (200 ng/mL for 5 min) causes higher phospho-c-Jun levels in all MEF cells, with wild-type phospho-c-Jun levels as high as in unstimulated TPC-deficient cells (Figure 9C). This result clearly indicates that TPC-deficient MEF cells already exhibit phospho-c-Jun levels that were achieved in wild-type cells only in the presence of EGF.

DISCUSSION

The intracellular trafficking network of the EGFR has been subject of numerous studies, and its understanding is of great value for establishing novel and innovative anti-tumor mechanisms (Sigismund et al., 2018). The network forms an ideal model system to study the functions of TPCs for regulation of receptor endocytosis, recycling, and degradation as well as for investigating receptor signaling. In our studies, we used high concentrations of EGF for receptor stimulation to achieve conditions that favor an uptake of EGFRs via CIE leading to lysosomal degradation of most activated receptor proteins (Caldieri et al., 2017). Owing to the preferred localizations of TPC1 in early and TPC2 in late endosomes and lysosomes (Calcraft et al., 2009; Castonguay et al., 2017), our single and double TPC-KO approach allowed us to discriminate between putatively different roles of TPCs in these endolysosomal compartments. The initial fluorescence microscopic studies—using Rab5 as a marker for early endosomes—demonstrated that TPC2- and TPC1/2-deficient MEF cells contained numerous vesicles that were positive for EGF and Rab5. In contrast, wild-type and TPC1-deficient cells showed much less co-localization of EGF and Rab5. These observations indicate that EGFR trafficking is delayed in TPC2-deficient cells. This may be caused by a longer retention time of the receptor in late endolysosomal compartments leading to a partial

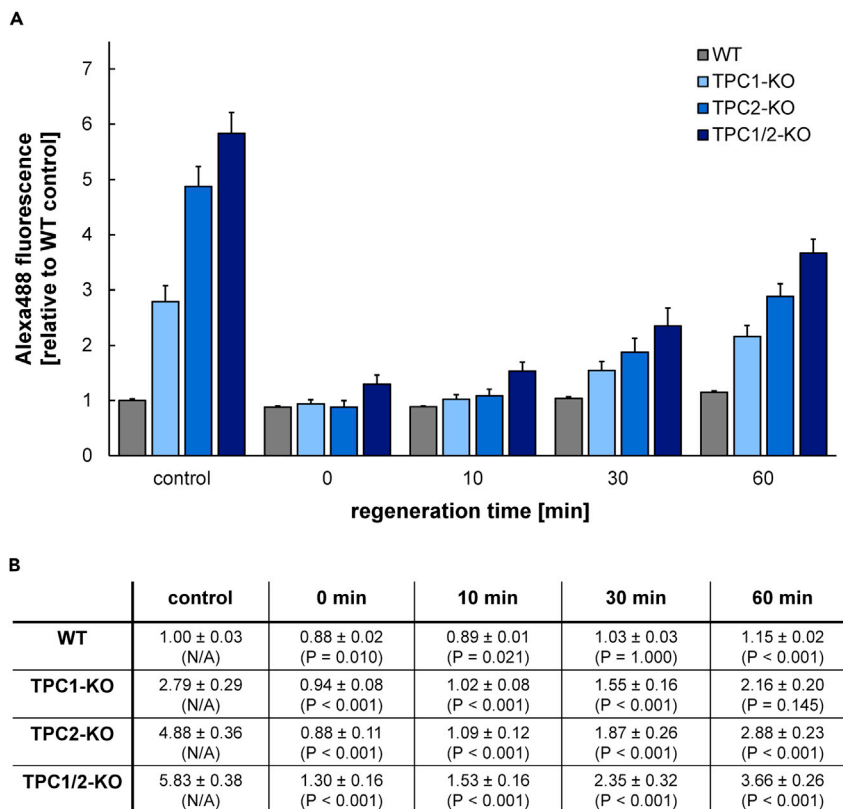


Figure 6. Regeneration rates of surface-accessible EGF receptor

(A) Bar diagram shows quantification of EGF-Alexa488 fluorescence signal for different regeneration periods ($t = 0$ min, $t = 10$ min, $t = 30$ min, and $t = 60$ min). Surface-accessible EGFRs were at first saturated with 200 ng/mL non-labeled EGF and then incubated with EGF-Alexa488. Control cells of each genotype were incubated with EGF-Alexa488 only. The corresponding bars indicate the initial levels of surface-accessible EGFRs. Bar diagram shows mean values and standard errors of the mean (SEM). Alexa 488 fluorescence intensities were normalized to wild-type values. Five independent experiments were performed ($n = 5$).

(B) Tabular display of measured values. Datasets were compared via ANOVA and Bonferroni post-hoc test for significance versus corresponding control value of each genotype (n.s., $p > 0.05$).

backlog of EGFR in early endosomes. In previous studies of TPC2-deficient cells, Grimm and colleagues performed co-localization experiments with the lysosomal marker LAMP-1 observing accumulation of EGFR in LAMP1-positive vesicles (Grimm et al., 2014). This also indicates a delay of receptor processing and trafficking and is in line with observations made in our experiments.

To gain additional insights into the time-dependent uptake of EGFRs, a FACS-based approach was chosen. Internalization of labeled EGF was quantified over an experimental window of 2 h. For each time point investigated, TPC1 and TPC2 single knockout cell lines demonstrated a 2- to 3-fold higher fluorescence signal than wild-type cells. For the TPC1/2-doubleKO the effect was additive and a 4- to 6-fold increase of EGF internalization was observed. These results are not limited to MEF cells and can be generalized due to our parallel studies with HeLa cells. Rescue experiments confirmed that the phenotype was indeed caused by deletion of TPCs. Re-expression of TPCs in corresponding knockout cells recovered the wild-type phenotype. These observations are in accordance with studies focusing on other model substrates such as LDL to monitor uptake of LDL receptor in TPC2-deficient cells (Grimm et al., 2014). Here, we add the finding that deletion of TPC1 also increases uptake of labeled substrate and that deletion of both channel subtypes causes an additive effect. We hypothesize that TPC1 and TPC2 meet spatial and/or timely diverse functions within the endolysosomal system. Having the specific distribution of the two TPC subtypes in mind (Calcraft et al., 2009; Castonguay et al., 2017) it seems likely that TPC1 is more important for receptor trafficking in early endosomes, whereas TPC2 contributes to transport processes from late endosomes to lysosomes.

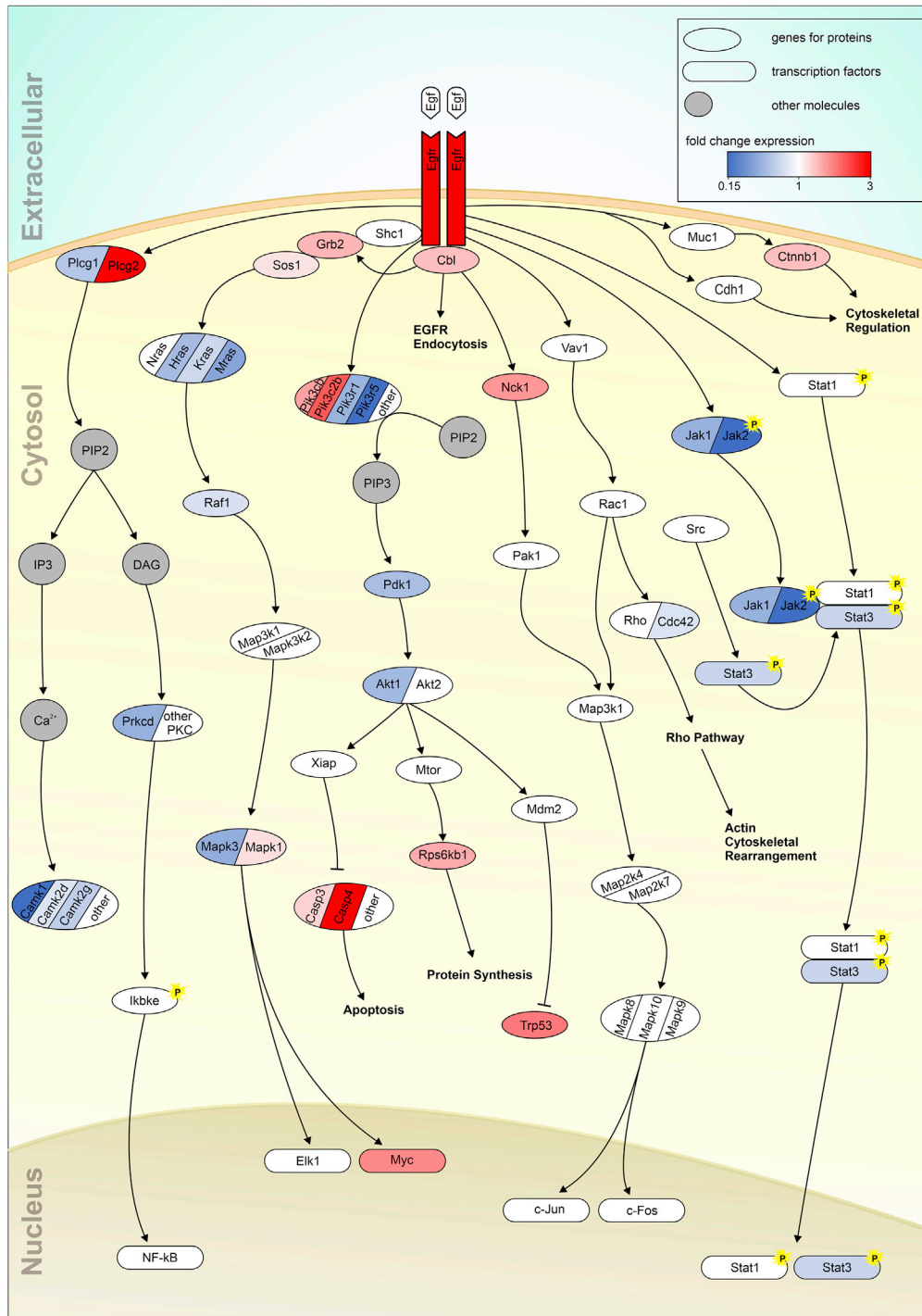


Figure 7. Differential gene expression of EGFR pathway proteins in TPC1-deficient MEF cells compared with wild-type cells

Color code indicates gradual changes in expression. Upregulated genes are displayed in red and downregulated genes are displayed in blue color. Genes that show no significant differential expression ($q > 0.05$) in RNA-seq of TPC1-KO versus wild-type MEF cells are shown in white (fold change 1, no difference). Figure was adopted from Brand et al. (2011).

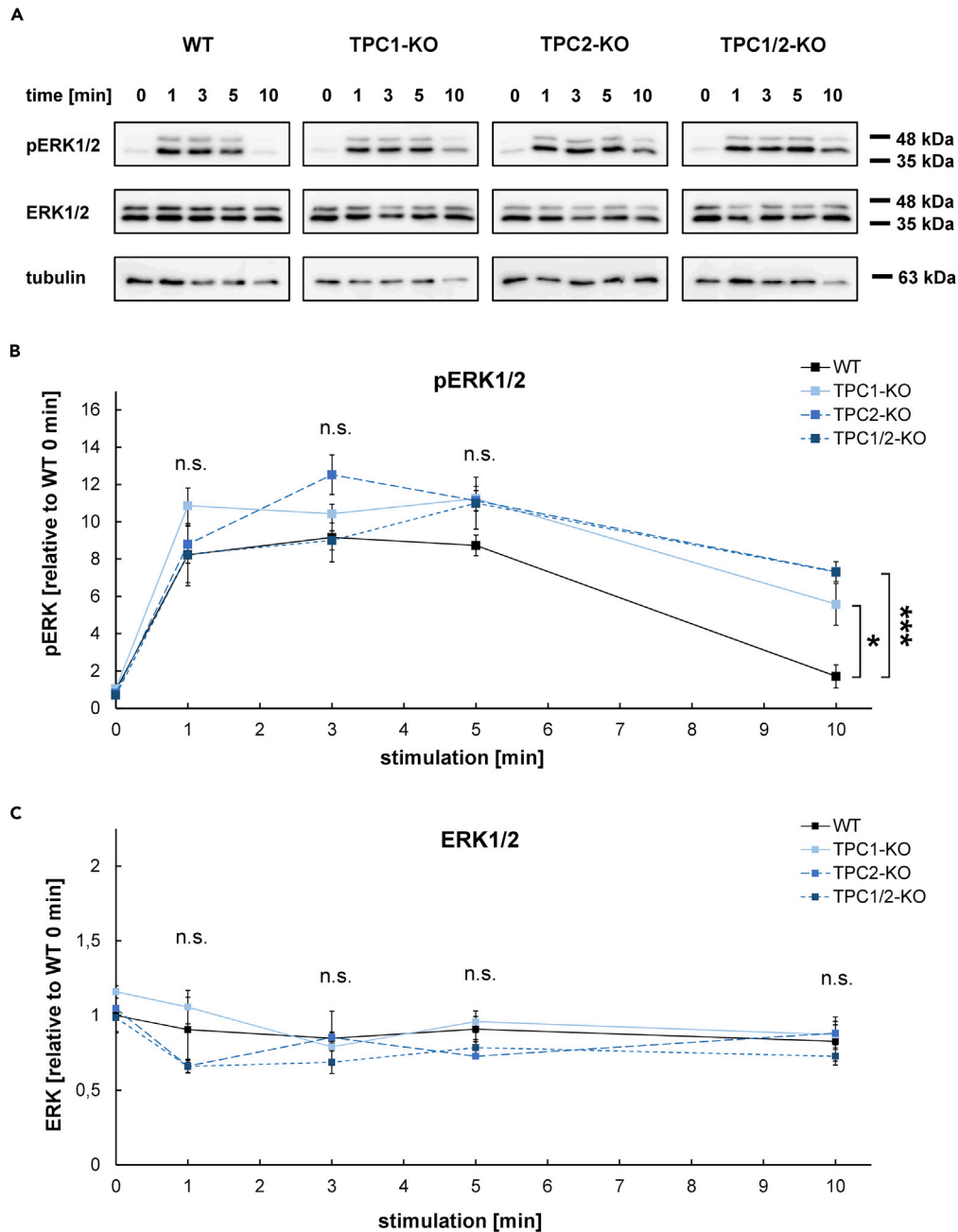


Figure 8. Quantification of total ERK1/2 and phosphorylated ERK1/2 (pERK1/2) after EGF stimulation

(A) Western blot analysis of pERK1/2 (top panel), total ERK1/2 (middle panel), and tubulin as control (bottom panel) in wild-type, TPC1-, TPC2-, and TPC1/2-deficient MEF cells after incubation with 200 ng/mL EGF for $t = 0$ min, $t = 1$ min, $t = 3$ min, $t = 5$ min, and $t = 10$ min.

(B) Time course and quantification of pERK1/2 levels from three independent experiments ($n = 3$).

(C) Time course and quantification of total ERK1/2 levels from three independent experiments ($n = 3$). (B and C) Datasets were compared via ANOVA and Bonferroni post-hoc test for significance versus wild-type control ($*p \leq 0.05$; $***p \leq 0.01$; n.s. $p > 0.05$).

Stability of the labeled EGF conjugate is of critical importance because premature lysosomal degradation would impair straightforward analysis of our EGFR trafficking studies. Therefore, we performed pulse-chase experiments with EGF-Alexa488 in MEF cells of all genotypes. In none of the cells, degradation or inactivation of the fluorophore occurred within 1 h and was not significantly different between the genotypes.

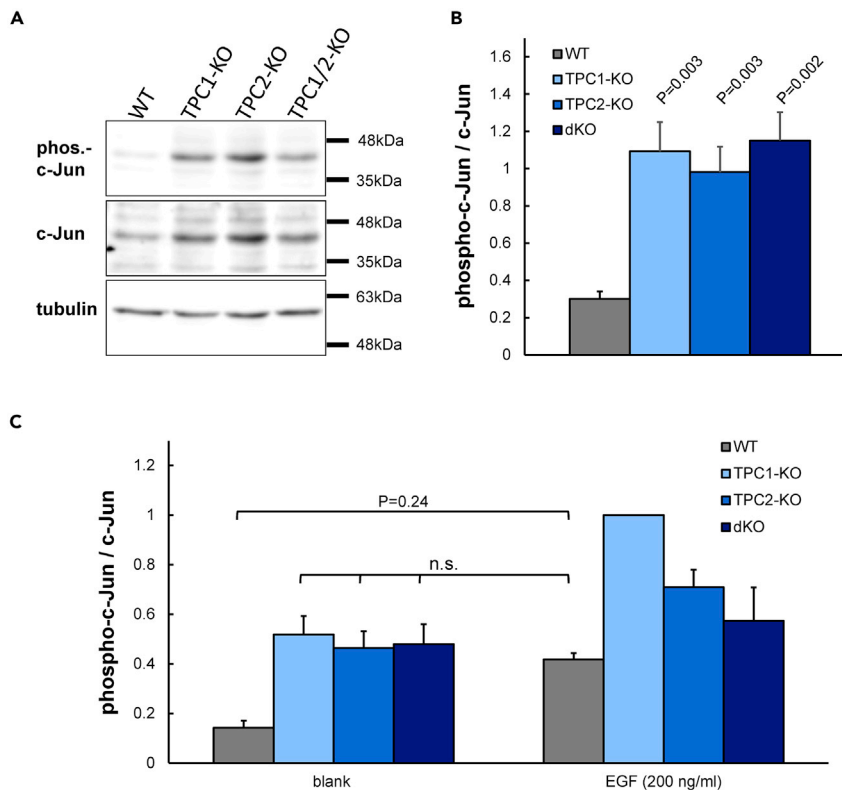


Figure 9. Phosphorylation of c-Jun under basal and EGF-stimulated conditions

(A) Representative example of basal phospho-c-Jun levels (top panel), total amount of c-Jun (middle panel), and tubulin loading control (bottom panel) in wild-type, TPC1-, TPC2- and TPC double knockout MEF cells.

(B) Quantification of six independent experiments presented as phospho-c-Jun/c-Jun relation ($n = 6$).

(C) Bar diagram demonstrating the phospho-c-Jun/c-Jun relation under basal (left) when compared with EGF-stimulated conditions (right) ($n = 3$).

Thus the observed differences between EGF-positive vesicles in wild-type and TPC-deficient cells cannot be attributed to lysosomal degradation of the Alexa 488 conjugate.

So far, our studies investigated the consequences of TPC deletion for the uptake of activated EGFR, but did not consider possible differences in the level of surface-expressed EGFR. Therefore, we quantified the amount of surface-expressed EGFRs and total EGFRs in MEF cells by receptor binding experiments and western blot analysis. The results for both approaches were rather comparable with an about 3-fold increase for TPC1-deficient cells, about 4-fold increase for TPC2-deficient cells, and 5- to 6-fold increase for TPC1/2-doubleKO cells. Again, these observations were not limited to MEF cells, but were also found in TPC1-deficient HeLa cells.

An altered degradation route might be one reason for the observed differences in *Egfr* expression levels and pointed us to compare the degradation kinetics of all genotypes. However, in the presence of a protein synthesis inhibitor no differences could be observed between all MEF cell lines. Therefore, the next studies were designed to discriminate between the two major regenerative mechanisms of receptor availability, recycling, and *de novo* protein biosynthesis. Quantification of surface-accessible EGFR was examined by binding of labeled EGF at low temperatures after saturation of receptors with non-labeled EGF. Regeneration rates were measured for up to 60 min at 37°C. To provide a comprehensive discussion of these studies it is necessary to analyze both the relative changes and the absolute fluorescence values. Wild-type cells had the capacity to reach the initial levels within 30 min, TPC1-deficient cells regenerated to about 80% after 1 h, and TPC2 and TPC1/2-doubleKO cells only achieved about 60% of the starting level. However, when considering the absolute amounts of surface-accessible EGFR levels, regeneration rates of all TPC knockouts were much higher than wild-type rates. Measurement of *egfr*-transcript levels supported these

findings and showed about 4-, 7- and 12-fold increases in TPC1-, TPC2-, and TPC1/2-doubleKO cells. RNA-seq analysis of *Egfr* transcripts from TPC1-deficient MEF cells also confirmed above-mentioned expression data. Taken together, these results suggest that EGFR *de novo* synthesis is the main mechanism responsible for the elevated levels of surface-accessible EGFR.

The strong increase of EGFR levels in TPC-deficient cells may have distinct consequences on EGFR-dependent signaling pathways. To get a first glimpse of changes in gene expression of EGFR pathway proteins following deletion of TPC1, we performed a detailed RNA-seq analysis when compared with wild-type cells. These data indicated numerous quantitative changes in the gene expression levels of EGFR pathway-related proteins, whereby up- and downregulation was observed. As these results did not favor a single candidate that would explain high EGFR expression, we additionally investigated phosphorylation of selected target proteins.

We analyzed ERK1/2 signaling by quantification of phosphorylated ERK1/2 (pERK1/2) in comparison in with total amounts of ERK1/2. Stimulation with EGF resulted in a fast increase of pERK1/2 levels in cells of all genotypes. In TPC-deficient cells ERK1/2 remained in the phosphorylated state for longer than 10 min. At this time, pERK1/2 levels already dropped down to initial non-stimulated levels in wild-type cells. These observations lead to the conclusion that TPC-deficient MEF cells exhibit prolonged EGFR signaling. Total amounts of non-phosphorylated ERK1/2 were unchanged throughout the entire experiment and were not different between the genotypes. Thus, massively increased EGFR expression in TPC-deficient cells does not account for a stronger or faster activation of EGFR, suggesting that the lower levels of EGFR in wild-type cells are already sufficient for maximal activation. A very similar effect was observed by means of a Ned-19 block of TPCs, which significantly increased and extended tyrosine phosphorylation of ERK1/2 (Kilpatrick et al., 2017).

Our studies indicate that deletion of TPCs does not only cause dysregulation of endolysosomal trafficking but also affects transcription of the *Egfr* gene and EGFR signaling. Therefore, we propose a new model linking function of TPCs with EGFR trafficking and signaling (Figure 10). Binding of EGF causes auto-cross-phosphorylation of the EGFR dimer and subsequent receptor activation. As of this time point, EGFR recruits downstream signaling complexes and triggers specific cellular signaling cascades. Noteworthy, EGFR signaling is ongoing as long as the receptor kinase domain is accessible from the cytosolic side (Conte and Sigismund, 2016; Wu et al., 2012). Comparable mechanisms have been reported for numerous other receptors that use endolysosomal compartments as major signaling platforms (Murphy et al., 2009). During maturation from early to late endosomes, EGFR is internalized in multivesicular bodies and receptor signaling is terminated. Ultimately, receptor and ligand degradation occurs in lysosomes. In this context, deletion of TPCs causes a delay of endolysosomal EGFR trafficking and thereby a prolonged EGFR signaling and continuous activation of associated signaling pathways. Exactly that was observed for phosphorylation of ERK1/2: pERK1/2 levels remained unchanged in TPC-deleted MEF cells for longer than 10 min, whereas pERK1/2 levels dropped down in wild-type cells to initial levels. If this mechanism holds true also for other EGFR-activated complexes, it can be hypothesized that further signaling pathways might be affected. Among them *c-Jun* is of particular interest because it has been shown to be a major factor for *Egfr*-gene transcription regulation (Fang et al., 2014; Mialon et al., 2005; Weston et al., 2004). We compared phospho-*c-Jun* levels in wild-type and TPC-deficient MEF cells and identified increased phospho-*c-Jun* levels in all cells lacking at least one functional TPC gene. Remarkably, this rise was already observable under unstimulated conditions. Thus, we hypothesize that the increased *JNK* signaling is a major factor that contributes to the high EGFR expression found in TPC-deficient cells. The prolonged EGFR signaling in endolysosomal compartments caused by deletion of TPCs most likely results in increased *JNK* signaling, which in turn leads to increased *Egfr* expression, ultimately forming a positive feedback loop. This positive feedback would be an explanation for the strongly increased amounts of surface accessible EGFRs found in TPC-deficient cells.

In summary, our work sheds light on a novel aspect of TPC function in the endolysosomal system. In addition to the well-known effects on trafficking, TPC deletions also influence gene transcription by ongoing receptor activation in endolysosomal compartments.

Limitations of the study

Our study was performed with MEF and HeLa cells, but not with primary cells. Particularly with regard to tumor cells, the expression of EGFR may vary within wide limits. We cannot rule out the possibility that in some tumors EGFR-related pathways may be affected in different ways.

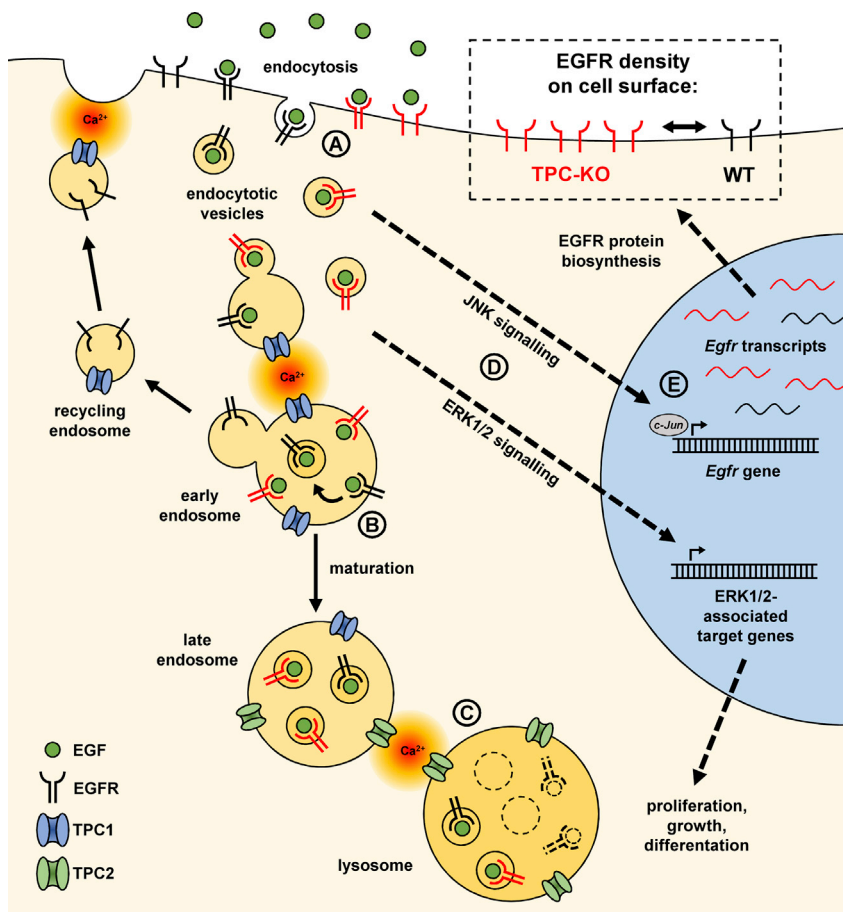


Figure 10. Model for the function of TPCs for EGFR trafficking and signaling

(A) Dimerization and auto-cross-phosphorylation of EGFR after binding of EGF and subsequent initiation of EGFR signaling. Following internalization of EGFR in endocytotic vesicles and fusion of vesicles to early endosomes, EGFR signaling is ongoing as long as intracellular part of EGFR is accessible from cytosol.
 (B) Maturation step of early to late endosomes and to multi-vesicular bodies, respectively. Internalization of EGFR into multi-vesicular bodies terminates EGFR signaling.
 (C) Late endosomes fuse with lysosomes where EGFR degradation occurs. During maturation from early endosomes to lysosomes the predominant TPC shifts from TPC1 to TPC2.
 (D) Activation of ERK1/2 signaling occurs as long as the receptor kinase domain is accessible from cytosol. Deletion of TPCs leads to a prolonged ERK phosphorylation and pERK signaling.
 (E) Deletion of TPCs leads to a comparable effect for JNK signaling pathways. Prolonged activation of c-Jun increases transcription of the *egfr* gene and number of surface-accessible EGFR.

Resource availability

Lead contact

Further information and requests for resources should be directed to and will be fulfilled by the Lead Contact, Norbert Klugbauer (n.klugbauer@pharmakol.uni-freiburg.de).

Materials availability

Materials generated in this study will be made available upon reasonable request and may require a material transfer agreement.

Data and code availability

Original sequencing data have been deposited in the Short Read Archive at the National Center for Biotechnology Information (NCBI) under the BioProject ID PRJNA694624. RNA-seq dataset generated in this study will be made available upon reasonable request.

METHODS

All methods can be found in the accompanying [Transparent Methods](#) supplemental file.

SUPPLEMENTAL INFORMATION

Supplemental information can be found online at <https://doi.org/10.1016/j.isci.2021.102099>.

ACKNOWLEDGMENTS

We thank Ute Christoph and Claudia Domisch for excellent technical assistance. We are grateful to Sami Hassan and Christian Grimm for providing the TPC2 knockout MEF cell line. This work was supported by the Deutsche Forschungsgemeinschaft, Germany DFG (Sachbeihilfe KL1119/6-1 (N.K)).

AUTHOR CONTRIBUTIONS

T.M., S.G., C.R., and R.T.M. performed the experiments. T.M., R.T.M., C.R., and N.K. conceived and designed the study. T.M., S.G., R.T.M., C.R., L.H., and N.K. analyzed and discussed the data. N.K. wrote the manuscript with input from all authors.

DECLARATION OF INTERESTS

The authors declare no competing interests.

Received: May 20, 2020

Revised: November 30, 2020

Accepted: January 20, 2021

Published: February 19, 2021

REFERENCES

- Arndt, L., Castonguay, J., Arlt, E., Meyer, D., Hassan, S., Borth, H., Zierler, S., Wennemuth, G., Breit, A., Biel, M., et al. (2014). NAADP and the two-pore channel protein 1 participate in the acrosome reaction in mammalian spermatozoa. *Mol. Biol. Cell* 25, 948–964.
- Bakker, J., Spits, M., Neeffjes, J., and Berlin, I. (2017). The EGFR odyssey - from activation to destruction in space and time. *J. Cell Sci.* 130, 4087–4096.
- Brand, T.M., Iida, M., Li, C., and Wheeler, D.L. (2011). The nuclear epidermal growth factor receptor signaling network and its role in cancer. *Discov. Med.* 12, 419–432.
- Calcraft, P.J., Ruas, M., Pan, Z., Cheng, X., Arredouani, A., Hao, X., Tang, J., Rietdorf, K., Teboul, L., Chuang, K.T., et al. (2009). NAADP mobilizes calcium from acidic organelles through two-pore channels. *Nature* 459, 596–600.
- Caldieri, G., Barbieri, E., Nappo, G., Raimondi, A., Bonora, M., Conte, A., Verhoef, L., Confalonieri, S., Malabarba, M.G., Bianchi, F., et al. (2017). Reticulon 3-dependent ER-PM contact sites control EGFR nonclathrin endocytosis. *Science* 356, 617–624.
- Castonguay, J., Orth, J.H.C., Muller, T., Sleman, F., Grimm, C., Wahl-Schott, C., Biel, M., Mallmann, R.T., Bildl, W., Schulte, U., et al. (2017). The two-pore channel TPC1 is required for efficient protein processing through early and recycling endosomes. *Sci. Rep.* 7, 10038.
- Ceresa, B.P., and Peterson, J.L. (2014). Cell and molecular biology of epidermal growth factor receptor. *Int. Rev. Cell Mol. Biol.* 313, 145–178.
- Conte, A., and Sigismund, S. (2016). Chapter six - the ubiquitin network in the control of EGFR endocytosis and signaling. *Prog. Mol. Biol. Transl. Sci.* 141, 225–276.
- Fang, Y., Wang, Y., Wang, Y., Meng, Y., Zhu, J., Jin, H., Li, J., Zhang, D., Yu, Y., Wu, X.R., et al. (2014). A new tumour suppression mechanism by p27Kip1: EGFR down-regulation mediated by JNK/c-Jun pathway inhibition. *Biochem. J.* 463, 383–392.
- Galione, A. (2019). NAADP receptors. *Cold Spring Harb. Perspect. Biol.* 11, a035071.
- Grimm, C., Chen, C.C., Wahl-Schott, C., and Biel, M. (2017). Two-pore channels: catalyzers of endolysosomal transport and function. *Front. Pharmacol.* 8, 45.
- Grimm, C., Holdt, L.M., Chen, C.C., Hassan, S., Muller, C., Jors, S., Cuny, H., Kissing, S., Schroder, B., Butz, E., et al. (2014). High susceptibility to fatty liver disease in two-pore channel 2-deficient mice. *Nat. Commun.* 5, 4699.
- Jentsch, T.J., Hoegg-Beiler, M.B., and Vogt, J. (2015). Departure gate of acidic Ca(2+)-confirmed. *EMBO J.* 34, 1737–1739.
- Kilpatrick, B.S., Eden, E.R., Hockey, L.N., Yates, E., Futter, C.E., and Patel, S. (2017). An endosomal NAADP-sensitive two-pore Ca(2+) channel regulates ER-endosome membrane contact sites to control growth factor signaling. *Cell Rep.* 18, 1636–1645.
- Marchant, J.S., and Patel, S. (2015). Two-pore channels at the intersection of endolysosomal membrane traffic. *Biochem. Soc. Trans.* 43, 434–441.
- Mialon, A., Sankinen, M., Soderstrom, H., Junttila, T.T., Holmstrom, T., Koivusalo, R., Papageorgiou, A.C., Johnson, R.S., Hietanen, S., Elenius, K., et al. (2005). DNA topoisomerase I is a cofactor for c-Jun in the regulation of epidermal growth factor receptor expression and cancer cell proliferation. *Mol. Cell Biol.* 25, 5040–5051.
- Murphy, J.E., Padilla, B.E., Hasdemir, B., Cottrell, G.S., and Bunnnett, N.W. (2009). Endosomes: a legitimate platform for the signaling train. *Proc. Natl. Acad. Sci. U S A* 106, 17615–17622.
- Patel, S. (2015). Function and dysfunction of two-pore channels. *Sci. Signal.* 8, re7.
- Rappoport, J.Z., and Simon, S.M. (2009). Endocytic trafficking of activated EGFR is AP-2 dependent and occurs through preformed clathrin spots. *J. Cell Sci.* 122, 1301–1305.
- Sakurai, Y., Kolokoltsov, A.A., Chen, C.C., Tidwell, M.W., Bauta, W.E., Klugbauer, N., Grimm, C., Wahl-Schott, C., Biel, M., and Davey, R.A. (2015). Ebola virus. Two-pore channels control Ebola virus host cell entry and are drug targets for disease treatment. *Science* 347, 995–998.
- Shan, Y., Eastwood, M.P., Zhang, X., Kim, E.T., Arkhipov, A., Dror, R.O., Jumper, J., Kuriyan, J., and Shaw, D.E. (2012). Oncogenic mutations counteract intrinsic disorder in the EGFR kinase and promote receptor dimerization. *Cell* 149, 860–870.
- Sigismund, S., Argenzio, E., Tosoni, D., Cavallaro, E., Polo, S., and Di Fiore, P.P. (2008). Clathrin-mediated internalization is essential for sustained

EGFR signaling but dispensable for degradation. *Dev. Cell* 15, 209–219.

Sigismund, S., Avanzato, D., and Lanzetti, L. (2018). Emerging functions of the EGFR in cancer. *Mol. Oncol.* 12, 3–20.

Sousa, L.P., Lax, I., Shen, H., Ferguson, S.M., De Camilli, P., and Schlessinger, J. (2012). Suppression of EGFR endocytosis by dynamin depletion reveals that EGFR signaling occurs

primarily at the plasma membrane. *Proc. Natl. Acad. Sci. U S A* 109, 4419–4424.

Tomas, A., Futter, C.E., and Eden, E.R. (2014). EGF receptor trafficking: consequences for signaling and cancer. *Trends Cell Biol.* 24, 26–34.

Vieira, A.V., Lamaze, C., and Schmid, S.L. (1996). Control of EGF receptor signaling by clathrin-mediated endocytosis. *Science* 274, 2086–2089.

Weston, C.R., Wong, A., Hall, J.P., Goad, M.E., Flavell, R.A., and Davis, R.J. (2004). The c-Jun NH2-terminal kinase is essential for epidermal morphogenesis. *Proc. Natl. Acad. Sci. U S A* 101, 14114–14119.

Wu, P., Wee, P., Jiang, J., Chen, X., and Wang, Z. (2012). Differential regulation of transcription factors by location-specific EGF receptor signaling via a spatio-temporal interplay of ERK activation. *PLoS One* 7, e41354.

iScience, Volume 24

Supplemental Information

**Two-pore channels affect EGF receptor
signaling by receptor trafficking
and expression**

**Thomas Müller, Sonja Grossmann, Robert Theodor Mallmann, Carolin Rommel, Lutz
Hein, and Norbert Klugbauer**

Supplemental Items

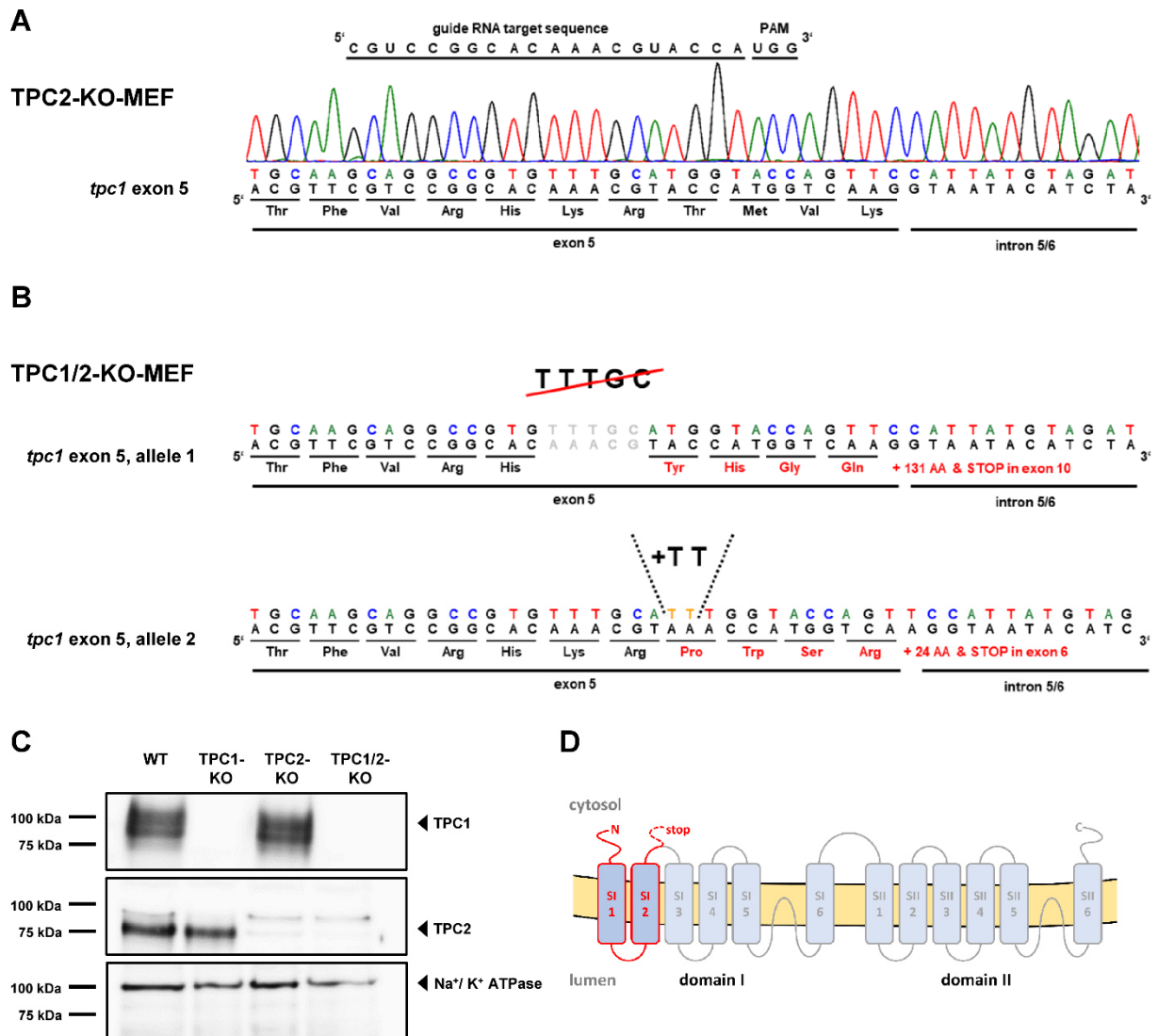


Figure S1. Generation of a TPC1/2 double knockout MEF cell line, Related to figure 1. A, A TPC2-deficient MEF cell line (TPC2-KO-MEF) was used to generate a TPC1/2 double KO line. Part of nucleotide and amino acid sequence of *tpc1* exon 5 and guide RNA target sequence. **B,** Sequence analysis of part of *tpc1* exon 5 after CRISPR Cas9-mediated gene targeting. Two events were observed, deletion of five base pairs (allele 1, TTTGC) and addition of two base pairs (allele 2, TT) in exon 5. Both mutations cause a frame shift and a premature stop codon. **C,** Western blot analysis to confirm inactivation of TPC genes in corresponding knockout cell lines. Immunoblot for TPC1 (upper line) and for TPC2 (middle line). Na⁺/K⁺-ATPase was used as a loading control (lower line). **D,** Scheme of TPC transmembrane and domain structure with N- and C-termini located in the cytosol. Red color indicates truncated TPC1-fragment as a result of CRISPR Cas9-mediated gene targeting of exon 5; only the first two transmembrane segments are generated.

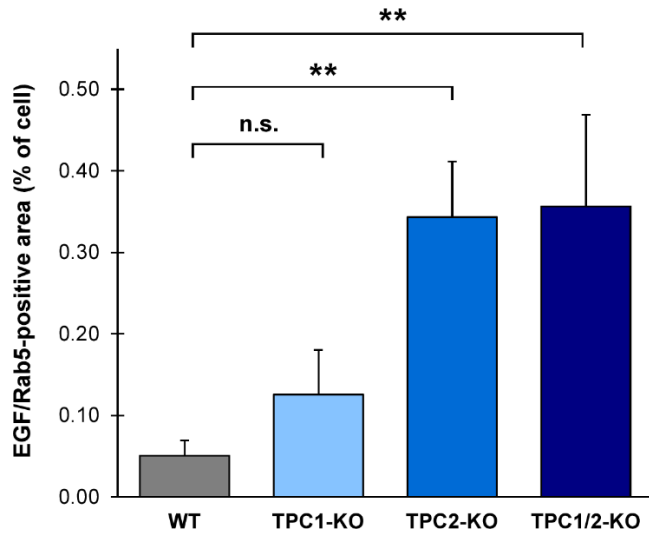


Figure S2. Co-localization analysis of EGF with Rab5 marker in MEF cells, Related to figure 1. The area covered by EGF/Rab5 positive vesicles relative to cell size is shown for each phenotype (n=10). One-way ANOVA was applied for statistical analysis. *** $P < 0.01$; ** $P < 0.03$; * $P < 0.05$; n.s. $P > 0,05$.

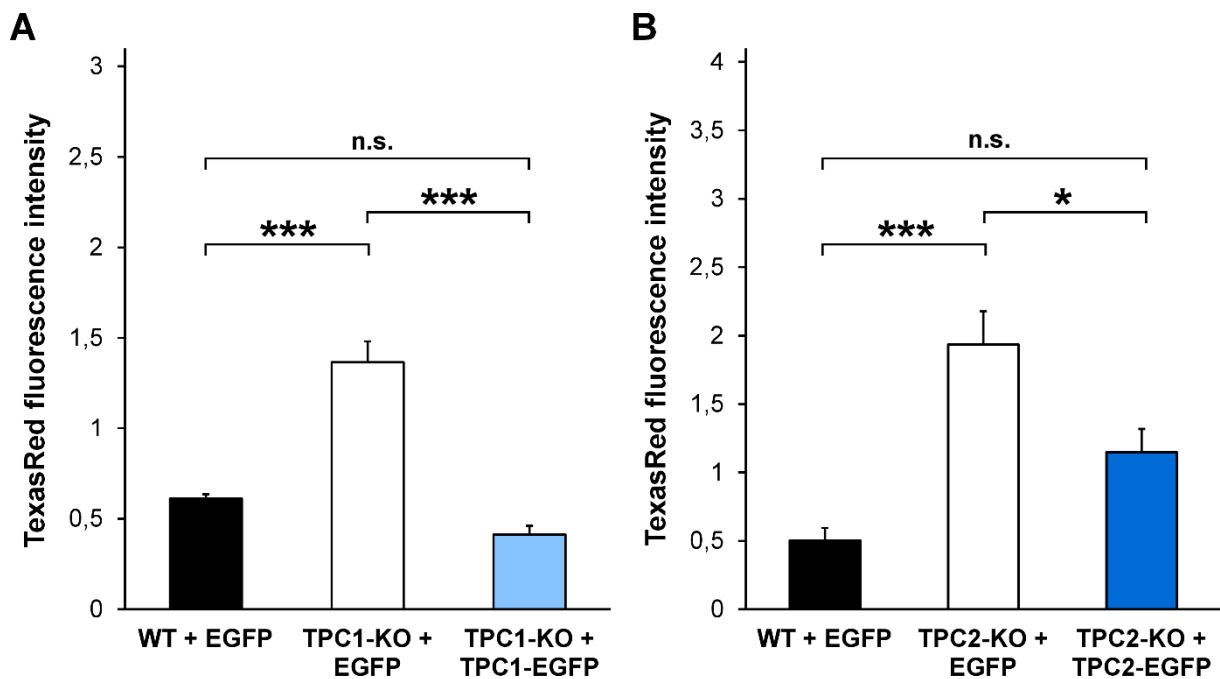


Figure S3. Rescue experiments demonstrating that transfection of corresponding TPC-EGFP plasmid reconstitutes wild type EGF-TexasRed fluorescence intensity, Related to figure 2. A, TPC1 rescue experiment measuring TexasRed fluorescence after two-hour incubation with EGF-TexasRed. Wild type and TPC1-knockout MEF cells were either transfected with EGFP or with TPC1-EGFP plasmid as indicated. Bar diagram shows mean values and standard errors of three independent

experiments (n = 3). WT+EGFP: 0.61 ± 0.02 . TPC1-KO+EGFP: 1.36 ± 0.12 . TPC1-KO+TPC1-EGFP: 0.41 ± 0.05 . Data sets were analyzed by ANOVA and student-Newman-Keuls Post-hoc test for significance (* $P \leq 0.05$; ** $P \geq 0.03$; *** $P \leq 0.01$; n.s. $P > 0.05$). P-values: WT+EGFP vs. TPC1-KO+EGFP $P = 0.001$; TPC1-KO+EGFP vs. TPC1-KO+TPC1-EGFP $P < 0.001$; WT+EGFP vs. TPC1-KO+TPC1-EGFP $P = 0.173$. **B**, same as **A**, but rescue experiment for TPC2 (n = 3). WT+EGFP: 0.50 ± 0.09 . TPC2-KO+EGFP: 1.93 ± 0.24 . TPC2-KO+TPC1-EGFP: 1.15 ± 0.29 . Data sets were analyzed by ANOVA and student-Newman-Keuls Post-hoc test for significance (* $P \leq 0.05$; ** $P \leq 0.03$; *** $P \leq 0.01$; n.s. $P > 0.05$). P-values: WT+EGFP vs. TPC2-KO+EGFP $P = 0.009$; TPC2-KO+EGFP vs. TPC2-KO+TPC1-EGFP $P = 0.044$; WT+EGFP vs. TPC1-KO+TPC2-EGFP $P = 0.084$.

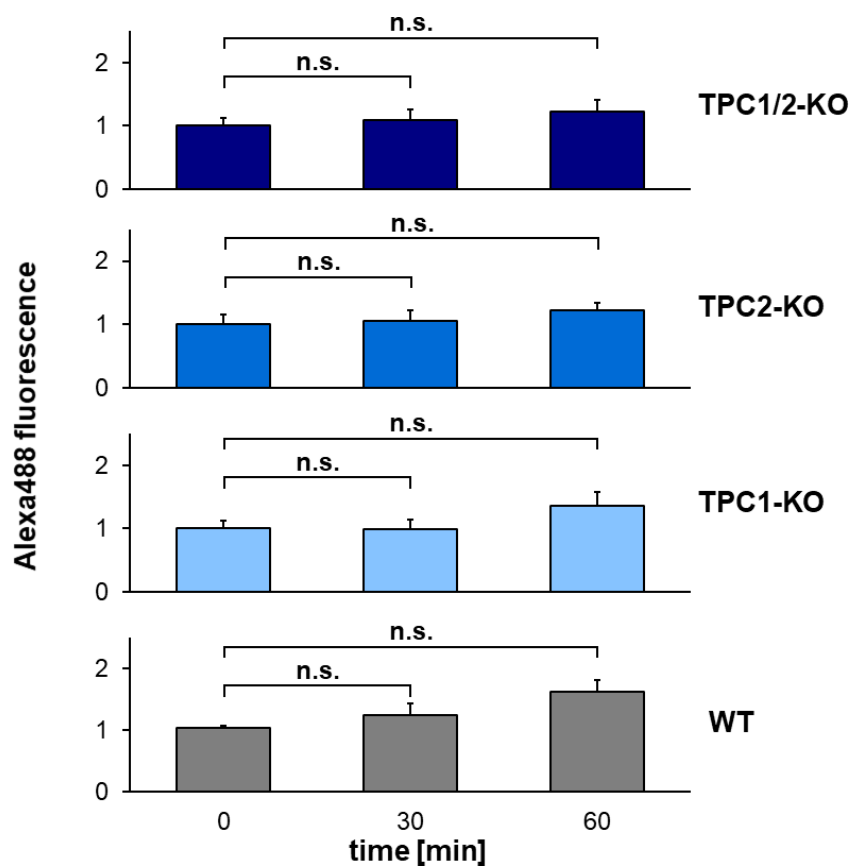


Figure S4. EGF-Alexa488 is not degraded in the endolysosomal system, Related to figure 2. Quantification of fluorescence intensity after a one-hour incubation with EGF-Alexa488 (t = 0 min) and subsequent treatment with EGF for 30 or 60 minutes. Bars show mean values and standard errors of the median Alexa488-fluorescence intensities normalized to the t = 0 min values. Data sets were collected from four independent experiments (n = 4) and analyzed by ANOVA and Bonferroni Post-hoc test for significance versus corresponding t = 0 min values.

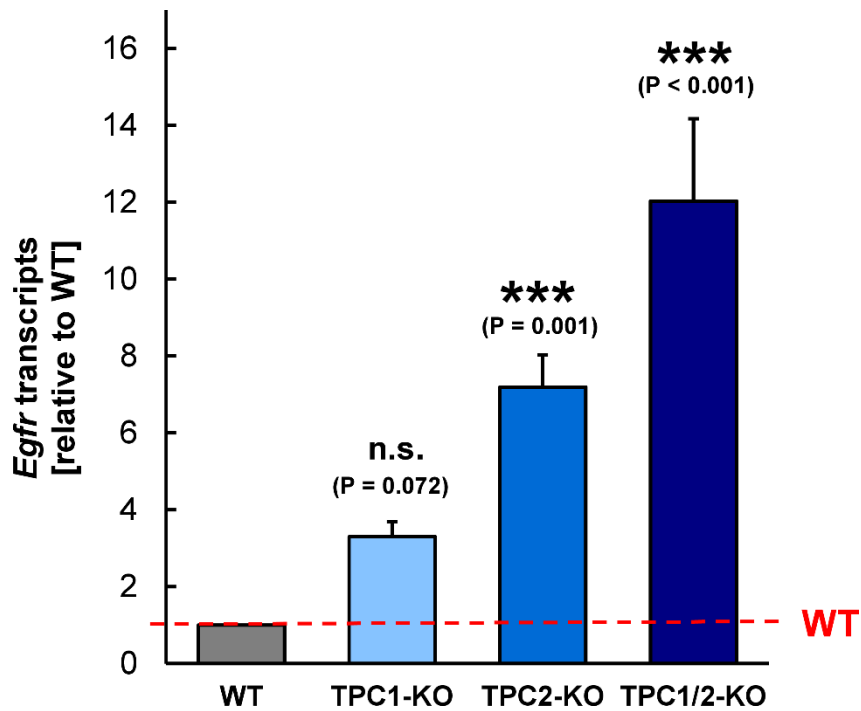


Figure S5. Quantification of *Egfr*-transcript levels in TPC-deficient MEF cell lines by *real-time-PCR*, Related to figure 6. Amounts of *egfr*-transcripts were normalized to actin transcript levels and are presented in relation to wild type level (red dotted line). Data were collected from nine independent experiments (n = 9). Δ CT-values of data sets were statistically analyzed by ANOVA with Bonferroni Post-hoc test to check for significance of wild type versus control group (***) $P \leq 0.01$; n.s. $P > 0.05$). TPC1-KO: 3.30 ± 0.38 ($P = 0.072$). TPC2-KO: 7.19 ± 0.85 ($P < 0.001$). TPC1/2-KO: 12.03 ± 2.13 ($P < 0.001$).

Figure S6. RNA sequencing coverage tracks for EGFR in WT and TPC1 knockout cells, Related to figure 7. (A) RNA sequencing coverage tracks for EGFR in WT (n = 3) and TPC1 knockout (n = 3) cells. (B) Bar diagram of the mean normalized counts.

gene	fold change	gene	fold change	gene	fold change	gene	fold change
Akt1	0.595	Cdc42	n.s.	Mras	0.474	Prkca	n.s.
Akt2	n.s.	Cdh1	n.s.	Mtor	n.s.	Prkcb	n.s.
Camk1	0.438	Ctnnb1	1.424	Muc1	n.s.	Prkcd	0.541
Camk1d	n.s.	Egfr	3.244	Myc	1.770	Prkce	n.s.
Camk1g	n.s.	Elk1	n.s.	Nck1	1.685	Prkcg	n.s.
Camk2a	n.s.	Fos	n.s.	Nfkb1	n.s.	Prkci	n.s.
Camk2b	n.s.	Grb2	1.483	Nfkb2	n.s.	Prkcg	n.s.
Camk2d	0.856	Hras	0.609	Nras	n.s.	Prkcz	n.s.
Camk2g	0.720	Ikbke	n.s.	Pak1	n.s.	Rac1	n.s.
Camk2n1	0.276	Jak1	0.544	Pdk1	0.623	Raf1	0.837
Camk2n2	0.433	Jak2	0.580	Pik3c2b	2.087	Rela	n.s.
Camk4	n.s.	Jun	n.s.	Pik3ca	n.s.	Relb	n.s.
Casp1	n.s.	Kras	0.773	Pik3cb	1.610	Rhoa	n.s.
Casp12	n.s.	Map2k4	n.s.	Pik3cd	n.s.	Rps6kb1	1.552
Casp14	n.s.	Map2k7	n.s.	Pik3cg	n.s.	Shc1	n.s.
Casp2	n.s.	Map3k1	n.s.	Pik3r1	0.559	Sos1	1.168
Casp3	1.286	Map3k2	n.s.	Pik3r2	n.s.	Src	n.s.
Casp4	5.714	Mapk1	1.208	Pik3r3	n.s.	Stat1	n.s.
Casp6	n.s.	Mapk10	n.s.	Pik3r4	n.s.	Stat3	0.760
Casp7	n.s.	Mapk3	0.525	Pik3r5	0.153	Trp53	1.880
Casp8	n.s.	Mapk8	n.s.	Pik3r6	n.s.	Vav1	n.s.
Casp9	n.s.	Mapk9	n.s.	Plcg1	0.674	Xiap	n.s.
Cbl	1.415	Mdm2	n.s.	Plcg2	2.835		

Table S1. Changes in gene expression levels of EGFR pathway proteins, Related to figure 7.

RNA sequencing analysis of selected genes involved in EGFR pathways in TPC1-KO vs. WT MEF cells, given as fold change. Genes that show no significant differential expression ($q > 0.05$) in TPC1-KO vs. WT MEF cells are marked as n.s.

A**pERK1/2**

	WT	TPC1-KO	TPC2-KO	TPC1/2-KO
0 min	1.00 ± 0.14 ---	1.07 ± 0.24 (n.s.)	0.81 ± 0.24 (n.s.)	0.70 ± 0.12 (n.s.)
1 min	8.23 ± 1.67 ---	10.86 ± 0.95 (n.s.)	8.79 ± 1.00 (n.s.)	8.25 ± 1.51 (n.s.)
3 min	9.16 ± 1.31 ---	10.44 ± 0.50 (n.s.)	12.52 ± 1.05 (n.s.)	9.00 ± 0.52 (n.s.)
5 min	8.73 ± 0.56 ---	11.24 ± 0.66 (n.s.)	11.13 ± 0.54 (n.s.)	11.00 ± 1.40 (n.s.)
10 min	1.71 ± 0.62 ---	5.58 ± 1.12 (P = 0.038)	7.33 ± 0.54 (P = 0.005)	7.30 ± 0.13 (P = 0.005)

B**ERK1/2**

	WT	TPC1-KO	TPC2-KO	TPC1/2-KO
0 min	1.00 ± 0.12 ---	1.16 ± 0.01 (n.s.)	1.05 ± 0.15 (n.s.)	0.99 ± 0.01 (n.s.)
1 min	0.91 ± 0.22 ---	1.06 ± 0.11 (n.s.)	0.66 ± 0.05 (n.s.)	0.66 ± 0.04 (n.s.)
3 min	0.85 ± 0.18 ---	0.79 ± 0.09 (n.s.)	0.85 ± 0.04 (n.s.)	0.69 ± 0.08 (n.s.)
5 min	0.91 ± 0.08 ---	0.96 ± 0.07 (n.s.)	0.73 ± 0.01 (n.s.)	0.79 ± 0.05 (n.s.)
10 min	0.83 ± 0.13 ---	0.87 ± 0.07 (n.s.)	0.88 ± 0.11 (n.s.)	0.73 ± 0.06 (n.s.)

Table S2. Phosphorylated ERK1/2 and total ERK1/2 (pERK1/2) levels after EGF stimulation, Related to figure 8. Western blot data were used to quantify the levels of (A) pERK1/2 and (B) ERK1/2 following stimulation by EGF for 1 min, 3 min, 5 min and 10 min. Presented data show mean values and standard errors of the Western blot signals from three independent experiments (n = 3) compared to untreated wild type cells (t = 0 min). Data sets of each time point were analyzed by ANOVA and Bonferroni Post-hoc test for significance towards wild type control groups. Significant differences are shown in red color; P-values are indicated in parentheses.

Transparent Methods

Cell lines. MEF cells and Hela cells were grown in DMEM (Biochrom) containing 10 % fetal calf serum (FCS) and 1 mM sodium pyruvate (PAA Laboratories) in an atmosphere of 5 % CO₂, and 95 % air at 37 °C. Cells were passaged using 0,05 % Trypsin/0,02 % EDTA in PBS without Ca²⁺ and Mg²⁺ (PAN-Biotech) every two to three days.

CRISPR/Cas9 genome editing. MEF TPC1/2-KO cells were created by means of CRISPR/Cas9 genome editing, following previously established methodologies (Zong et al., 2009). Candidate gRNA target sequences were identified with the MIT CRISPR Design Tool (crispr.mit.edu). Target sequence in *tpc1* gene exon 5: CGTCCGGCACAAACGTACCA. The pSpCas9(BB)-2A-Puro vector containing the gRNA target sequence was used for transfection of MEF TPC2-KO cells. Selection of successfully transfected cells was achieved with addition of puromycin into growth media. Single cells were isolated to ensure a clonal origin of the TPC1/2-KO cell line. The knockout of TPC1 was confirmed on DNA and protein level via sequencing of *tpc1* gene and immunoblot analysis.

Confocal Microscopy. MEF cells were seeded on HCl-washed glass coverslips in 24-well plates one day prior to the experiment and grown to a confluence of 60 to 80 % overnight. Cultivation medium was replaced by serum free growth medium and MEF cells were treated with 200 nM Alexa Fluor™ 488 EGF complex (Thermo Fisher Scientific) for 60 minutes at 37° C. The cells were washed with PBS and fixated with 4 % paraformaldehyde / PBS for 20 minutes at room temperature. For immunocytochemical staining, cells were permeabilized with 0.15 % Triton-X100 / PBS for 20 minutes. Unspecific antigens were blocked with 1% BSA / 4% NGS / PBS overnight. For detection of Rab5 protein adequate primary and Alexa568® coupled secondary antibodies were used (see below list of antibodies). After washing with PBS, cells were mounted on microscope slides using ProLong™ Diamond Antifade Mountant + DAPI (Thermo Fisher Scientific). Images were acquired utilizing a Zeiss 200M confocal microscope equipped with a CSU-X1 Spinning Disc (Yokogawa). Images were post processed and analyzed with ImageJ software (NIH Maryland). For quantification of co-localization, borders of single cells were designated with the freehand selection tool. Cell sizes were calculated. For intracellular particle analysis binary images were created. Thresholds for analysis were set manually by adjusting the particular threshold for Rab5-marker for each image. In a second step threshold for EGF channel was adjusted. The binary image channels were merged and all non-overlapping signals excluded. EGF/Rab5-positive vesicles were counted utilizing the particle analysis tool. The area covered by EGF/Rab5-positive vesicles relative to cell size was calculated. One-way ANOVA was applied for statistical analysis.

Quantitative PCR. MEF cells were grown to a confluence of approximately 80 % in 6-well plates and incubated in serum free growth medium for 2 hours at 37 °C prior to each experiment. Messenger RNA was isolated from cells utilizing the RNeasy Midi Kit (Quiagen). The mRNA was subsequently rewritten into cDNA using the Transcriptor High Fidelity cDNA Synthesis Kit (Roche). EGFR and actin transcript amounts were analyzed by quantitative PCR. The Experiment was performed in the

Mastercycler®Realplex (Eppendorf) with GoTaq qPCR Master-Mix (Promega). Experimental data was analyzed with the Mastercycler®Realplex Software (Eppendorf). Expression levels of EGFR in TPC deficient cells were calculated utilizing the $\Delta\Delta CT$ method: $\Delta CT = CT(EGFR) - CT(Actin)$; $\Delta\Delta CT(KO/WT) = \Delta CT(KO) - \Delta CT(WT)$. The following primer pairs were used for qPCR experiments: bAct-qPCR-for (TCCTATGTGGGTGACGAGGCC) + bAct-qPCR-rev (TCACGGTTGGCCTTAGGGTTCAG); EGFR-qPCR-for (TGCTGGGCCAGGTCTTCAAGGA) + EGFR-qPCR-rev (TGGAGCTTCTCCGCTGGGTGTG). Primer pair efficiency was tested by creating cDNA dilution series from 1:1 to 1:10000 and subsequently performing qPCR analysis with each primer pair. Corresponding CT values were calculated and primer pair efficiency determined by logarithmic regression.

RNA sequencing. Total RNA was isolated from 3 independent samples of WT (n=3) and TPC1-KO MEF cells (n=3) using the RNeasy Micro Kit (Qiagen). For RNA sequencing amplified cDNA was prepared from 5 ng of total RNA according to the manufacturer's protocol (Ovation® SoLo RNA-Seq, NuGen®). 11-14 PCR cycles were used for library enrichment. Agencourt® AMPure® XP Beads (Beckman Coulter) were used for purification. Sequencing was carried out on NextSeq 500 (80 bp PE, Illumina®). Tools integrated in the Galaxy platform (Afgan et al., 2016) were used for computational analysis of sequencing data. Adaptor and quality trimming were performed and sequencing reads were mapped to the mouse genome assembly mm9 using RNA STAR (Dobin et al., 2013). Quality control, normalization and genome-wide visualization were performed with DeepTools (Ramirez et al., 2016). To remove potential PCR duplicates RmDup (Li et al., 2009) was performed. Htseq-count (Anders et al., 2015) followed by DESeq2 (Love et al., 2014) was used for differential gene expression analysis. A p-value and a false discovery rate (FDR) <0.05 was considered statistically significant. Annotations and genome files (mm9) were obtained from the UCSC genome browser (Karolchik et al., 2014). An EGFR Pathway Map was created with CoreIDRAW Graphics Suite 2020®.

ERK1/2 phosphorylation experiments. Mouse embryonic fibroblasts (MEF) were seeded into 6-well plates with 1 ml of medium 18 hours before the experiment. The cells were incubated in serum free growth medium for 2 hours at 37 °C. MEFs were exposed to 200 ng/ml EGF for 1, 3, 5 or 10 minutes at 37° C and immediately lysed with RIPA Buffer (137.5 mM NaCl, 50 mM Tris/HCl, 0.5 mM EDTA, 1 % Triton-X100, 1 % glycerol, 0.5 % sodium deoxycholate, 0.1 % SDS) after treatment. The samples were subjected to SDS-PAGE and transferred onto polyvinylidene difluoride (PVDF) membrane using the Trans-Blot® system (BioRad). ERK1/2, phosphorylated ERK1/2 (pERK1/2) and tubulin proteins were detected with respective primary antibody and appropriate horseradish peroxidase-coupled secondary antibody (see below list of antibodies). Immunoblots were analyzed using SignalFire™ ECL reagent (Cell Signaling) and the LAS-3000 mini image system (Fujifilm). Quantification of bioluminescence signal was performed with MultiGauge V3.0 software (Fujifilm).

c-Jun phosphorylation experiments. Mouse embryonic fibroblasts (MEF) were seeded into 6-well plates with 1 ml of medium 18 hours before the experiment. Cells were starved in serum free growth

medium for 6 hours at 37 °C and exposed to 200 ng/ml EGF for 5 minutes at 37°C. Following EGF-treatment, cells were lysed with ice-cold RIPA Buffer substituted with phosphatase-inhibitor cocktail 2 & 3 (Sigma). Samples were diluted 1:1 with 2x Laemmli Buffer and stored at -20°C or subjected to SDS-PAGE and transferred onto polyvinylidene difluoride (PVDF) membrane using the Trans-Blot® system (BioRad). Quantification of bioluminescence signal was performed with MultiGauge V3.0 software (Fujifilm).

Membrane preparations. For membrane preparations of cultured fibroblasts, MEF cells were seeded into 10 cm cell culture dishes. MEFs were grown to a confluence of approximately 80 %. The cultivation medium was removed, 500 µl PBS + cComplete™ buffer was added and cells were scraped from culture dish surface. Plasma membranes were further disintegrated by pulling cell suspensions through Ø0.45 mm cannula (3 cycles, each 10 times). Samples were centrifuged at 800 g for 10 minutes at 4 °C. Supernatants were rescued and subjugated to centrifugation at 2000 g for 10 minutes at 4 °C. In a third step, supernatants were centrifuged at 16000 g for 2 hours at 4 °C. The membrane pellets were shock frozen in liquid nitrogen and stored at -20 °C until further analysis.

Immunoblot analysis. For immunoblotting, protein samples were dissolved in 4M urea containing SDS sample buffer (250 mM Tris/HCl, 12.5 % glycerol, 2 % SDS, 0.0005 % bromophenol blue, 2.5 % β-mercaptoethanol). Protein content was determined utilizing the RC DC™ Protein Assay Kit (Bio Rad) and adjusted to an over-all protein concentration of 0,5 µg/µl. Proteins were separated by standard SDS-polyacrylamide gel electrophoresis (SDS-PAGE) on 7% or 12 % SDS-polyacrylamide gels. Unless specifically mentioned in corresponding figures, 10 µg over-all protein was loaded per lane. Proteins were transferred onto polyvinylidene difluoride (PVDF) membranes (Carl Roth®) using the Trans-Blot® system (BioRad). TPC1, TPC2, H⁺/K⁺-ATPase, tubulin and EGFR proteins were detected with respective primary antibody and appropriate horseradish peroxidase-coupled secondary antibody (see below list of antibodies). Immunoblots were analyzed using SignalFire™ ECL reagent (Cell Signaling) and the LAS-3000 mini image system (Fujifilm). Quantification of bioluminescence signal was performed with MultiGauge V3.0 software (Fujifilm).

EGFR degradation experiments. Mouse embryonic fibroblasts were seeded into 6-well plates one day prior to the experiment. The cells were incubated in serum free media for 2 hours at 37° C. Starved cells were pre-treated with serum free media containing 10 µg/ml cycloheximide (Carl Roth) for 20 minutes to block *de-novo* protein synthesis. The cells were exposed to 200 ng/ml EGF for 0, 15, 45, 90, 120 minutes at 37° C in the presence of 10 µg/ml cycloheximide. Control cells were stimulated with EGF for 120 minutes without cycloheximide. After treatment, cells were immediately washed with ice-cold PBS and lysed with RIPA buffer (137.5 mM NaCl, 50 nM Tris/HCl, 0.5 mM EDTA, 1 % Triton-X100, 1 % glycerol, 0.5 % sodium deoxycholate, 0.1 % SDS), frozen in liquid nitrogen and stored at -20° C until they were subjected to immunoblot analysis.

Antibodies

List of used antibodies with designation, target structure and reference

designation	target structure	reference
sc-1694	c-Jun	Santa Cruz Biotechnology
#3270	phospho-c-Jun (Ser73)	Cell Signalling
ab52894	EGFR	Abcam
sc-271269	ERK1	Santa Cruz Biotechnology
#9101	Phospho-p44/42 MAPK	Cell signalling
ab7671	H ⁺ /K ⁺ -ATPase	Abcam
#3827	TPC1	Arndt et al., 2014
#4913a	TPC2	Grimm et al., 2014
sc-598	Rab5	Santa Cruz Biotechnology
sc-23950	Tubulin	Santa Cruz Biotechnology
7076S	Mouse IgG, HRP coupled	New England Biolabs
7074S	Rabbit IgG, HRP coupled	New England Biolabs
A-11011	Rabbit IgG, Alexa Fluor 568 coupled	Thermo Fisher Scientific

Flow Cytometry. MEF or Hela cells were seeded into 6-well plates and grown to a confluence of approximately 80 %. Cultivation medium was replaced by serum free growth medium in which cells were incubated for 2 hours at 37 °C prior to each experiment.

Adhesion experiments: MEF cells were cooled down to 4°C and washed with cold PBS three times. Cells were treated with 200 ng/ml Alexa Fluor™ 488 EGF complex (Thermo Fisher Scientific) in PBS for 60 minutes at 4° C. Untreated cells served as a control group to determine baseline fluorescence. After washing three times with cold PBS, cells were detached from culture dish surface with 100 µM EDTA / PBS and stored in light-tight Eppendorf tubes on ice until flow cytometrical analysis.

Uptake experiments: MEF or Hela cells were treated with 200 ng/ml Alexa Fluor™ 488 EGF complex (Thermo Fisher Scientific) in serum free growth medium for 10, 30, 60, 120 or 180 minutes at 37° C. Untreated cells served as a control group to determine baseline fluorescence. The uptake was stopped by removing EGF containing medium and washing with ice-cold PBS three times. Cells were detached from culture dish surface with 100 µM EDTA / PBS and stored in light-tight Eppendorf tubes on ice until flow cytometrical analysis.

Regeneration experiments: MEF cells were cooled down to 4°C and washed with cold PBS three times. MEF cells were treated with 200 ng/ml EGF in serum free growth medium for 60 minutes at 4° C. Cells were washed with cold PBS three times and treated with 200 ng/ml Alexa Fluor™ 488 EGF complex (Thermo Fisher Scientific) in serum free growth medium for 0, 10, 30 and 60 minutes at 37° C. The uptake was stopped by removing EGF containing medium and washing with ice-cold PBS three times.

Cells were detached from culture dish surface with 100 μ M EDTA / PBS and stored in light-tight Eppendorf tubes on ice until flow cytometrical analysis. As a positive control MEF cells were treated with 200 ng/ml Alexa Fluor™ 488 EGF complex for 60 minutes at 4 °C, washed 3 times with cold PBS and were directly analyzed after detachment from culture dish surface. An analysis of untreated cells was performed to determine baseline fluorescence.

Rescue experiments: One day prior to the experiment TPC deficient MEF cells were transfected with a corresponding GFP labeled TPC construct. Additionally, control samples were transfected with a GFP expressing vector. Wild type MEF cells transfected with GFP vector served as a control. Mouse embryonic fibroblasts were grown to a confluence of 60 -80 % and incubated in serum free growth medium for 2 hours at 37 °C prior to the experiment. Cells were washed with PBS and serum free medium was added. MEF cells were treated with 200 ng/ml TexasRed™ EGF complex (Thermo Fisher Scientific) in serum free growth medium for 120 minutes at 37° C. The uptake was stopped by removing EGF containing medium and washing with ice-cold PBS three times. Cells were detached from culture dish surface with 100 μ M EDTA / PBS and stored in light-tight Eppendorf tubes on ice until flow cytometrical analysis.

Flow cytometrical analysis: All samples were analyzed with a FACSMelody™ (BD Biosciences) flow cytometer. The FlowJo® Software (LLC) was used for data processing. Forward scatter versus side scatter density plots were analyzed and the main population of cells was gated for each data set. Alexa Fluor™ 488 fluorescence histograms of selected cell populations were created and the median fluorescence intensities were calculated.

For Rescue experiments, exclusively cells that showed transfection with either control construct or GFP labeled TPC channels were considered for analysis. For this purpose, an additional gating step was performed after selection of main populations. Cells that showed merely baseline GFP fluorescence were excluded from data sets. Afterwards fluorescence histograms of the gated main cell populations were created and the median TexasRed™ fluorescence intensities were calculated.

Statistics and reproducibility. All experiments were independently repeated at least three times. The exact number of experimental repetitions (n) is shown in each figure legend. All data are presented as mean \pm SEM. Sigma Plot software (Systat) was used for statistical analysis. Unless specifically mentioned, a one-way ANOVA with Bonferroni post-hoc test was performed to determine statistical significance of datasets. P values < 0,05 were considered significant.

Supplemental References

- Afgan, E., Baker, D., van den Beek, M., Blankenberg, D., Bouvier, D., Cech, M., Chilton, J., Clements, D., Coraor, N., Eberhard, C., *et al.* (2016). The Galaxy platform for accessible, reproducible and collaborative biomedical analyses: 2016 update. *Nucleic Acids Res* *44*, W3-W10.
- Anders, S., Pyl, P.T., and Huber, W. (2015). HTSeq--a Python framework to work with high-throughput sequencing data. *Bioinformatics* *31*, 166-169.
- Dobin, A., Davis, C.A., Schlesinger, F., Drenkow, J., Zaleski, C., Jha, S., Batut, P., Chaisson, M., and Gingeras, T.R. (2013). STAR: ultrafast universal RNA-seq aligner. *Bioinformatics* *29*, 15-21.
- Karolchik, D., Barber, G.P., Casper, J., Clawson, H., Cline, M.S., Diekhans, M., Dreszer, T.R., Fujita, P.A., Guruvadoo, L., Haeussler, M., *et al.* (2014). The UCSC Genome Browser database: 2014 update. *Nucleic Acids Res* *42*, D764-770.
- Li, H., Handsaker, B., Wysoker, A., Fennell, T., Ruan, J., Homer, N., Marth, G., Abecasis, G., Durbin, R., and Genome Project Data Processing, S. (2009). The Sequence Alignment/Map format and SAMtools. *Bioinformatics* *25*, 2078-2079.
- Love, M.I., Huber, W., and Anders, S. (2014). Moderated estimation of fold change and dispersion for RNA-seq data with DESeq2. *Genome Biol* *15*, 550.
- Ramirez, F., Ryan, D.P., Gruning, B., Bhardwaj, V., Kilpert, F., Richter, A.S., Heyne, S., Dundar, F., and Manke, T. (2016). deepTools2: a next generation web server for deep-sequencing data analysis. *Nucleic Acids Res* *44*, W160-165.
- Zong, X., Schieder, M., Cuny, H., Fenske, S., Gruner, C., Rotzer, K., Griesbeck, O., Harz, H., Biel, M., and Wahl-Schott, C. (2009). The two-pore channel TPCN2 mediates NAADP-dependent Ca²⁺-release from lysosomal stores. *Pflugers Arch* *458*, 891-899.